

Dynamics of entangled linear polymer melts: A molecular-dynamics simulation

Cite as: J. Chem. Phys. **92**, 5057 (1990); <https://doi.org/10.1063/1.458541>

Submitted: 10 October 1989 • Accepted: 26 December 1989 • Published Online: 31 August 1998

Kurt Kremer and Gary S. Grest



View Online



Export Citation

ARTICLES YOU MAY BE INTERESTED IN

[Dissipative particle dynamics: Bridging the gap between atomistic and mesoscopic simulation](#)

The Journal of Chemical Physics **107**, 4423 (1997); <https://doi.org/10.1063/1.474784>

[Erratum: Dynamics of entangled polymer melts: A molecular-dynamics simulation \[J. Chem. Phys. **92**, 5057 \(1990\)\]](#)

The Journal of Chemical Physics **94**, 4103 (1991); <https://doi.org/10.1063/1.460746>

[Molecular dynamics simulation of a polymer chain in solution](#)

The Journal of Chemical Physics **99**, 6983 (1993); <https://doi.org/10.1063/1.465445>

Learn More

The Journal
of Chemical Physics **Special Topics** Open for Submissions

Dynamics of entangled linear polymer melts: A molecular-dynamics simulation

Kurt Kremer

*Institut für Festkörperforschung, Forschungszentrum Jülich, D-5170 Jülich, West Germany^{a)}
and Institut für Physik, Universität Mainz, D-6500 Mainz, West Germany*

Gary S. Grest

Corporate Research Science Laboratory, Exxon Research and Engineering Company, Annandale, New Jersey 08801

(Received 10 October 1989; accepted 26 December 1989)

We present an extensive molecular-dynamics simulation for a bead spring model of a melt of linear polymers. The number of monomers N covers the range from $N = 5$ to $N = 400$. Since the entanglement length N_e is found to be approximately 35, our chains cover the crossover from the nonentangled to the entangled regime. The Rouse model provides an excellent description for short chains $N < N_e$, while the dynamics of the long chains can be described by the reptation model. By mapping the model chains onto chemical species we give estimates of the times and distances of onset of the slowing down in motion due to reptation. Comparison to neutron spin-echo data confirm our mapping procedure, resolving a discrepancy between various experiments. By considering the primitive chain we are able to directly visualize the confinement to a tube. Analyzing the Rouse mode relaxation allows us to exclude the generalized Rouse models, while the original reptation prediction gives a good description of the data.

I. INTRODUCTION

The physics of polymeric liquids has been a problem of considerable interest in recent years.¹⁻⁴ In contrast to liquids of small molecules, polymeric liquids display a rich and unusual viscoelastic behavior for time and distance scales, where ordinary liquids are still Newtonian.^{2,4} (For a review of the experimentally observed viscoelastic properties of polymers, we refer the reader to the classic books of Ferry³ and Bird *et al.*⁴, as well as more recent articles by Pearson⁵ and Graessley.⁶) The reason for this unusual behavior of polymeric liquids is that the motion of a polymer is subject to complicated topological constraints. Unlike simple atomic or molecular systems, long "entangled" chain polymers have to move in specific ways which are limited by the fact that they are connected to other monomers and they cannot cut through each other. It is the main concern of the present paper to investigate this motion in detail and compare our results to previous numerical investigations as well as to theoretical predictions and experiments. Although experiments have been very important in elucidating many of the interesting properties of these complex systems, there remain many unanswered questions. In particular, there has been no experiment up to now which is able to study directly the microscopic origin of the macroscopic effects which are observed. For this reason, computer simulations of highly entangled polymers can play an important role in our understanding of dense polymer melts. The aim of such a simulation should be to bridge the gap between experimental and analytical investigations and to provide a direct connection from a microscopic model of the motion to experimentally observable quantities. So far this has not been achieved. In this paper, we present a large-scale molecular-dynamics

(MD) simulation of a dense melt of linear polymers, which covers the range from the short nonentangled (Rouse^{1,7}) regime up to the highly entangled (reptation^{1,2,8-10}) regime. A short account summarizing some of the important aspects of this work has appeared in Ref. 11.

The dynamics of polymeric liquids are typically described in terms of the Rouse and reptation models.^{1,2} For short chains the topological constraints do not play a dominant role. For a given chain, the presence of the other chains can be accounted for as a stochastic background. The dynamics of the chain can then be described by a Langevin equation with noise and the constraint that the monomers are connected to form a chain. This results in the well-known Rouse behavior for the diffusion constant and viscosity. While there remain a few questions about the short-time behavior, this model describes the long-time behavior very well.^{1,2,12-16} The largest relaxation time $\tau_N \sim N^2$ where N is the number of bonds per chain. The diffusion constant $D \sim N^{-1}$ and the viscosity $\eta \sim N$. Experimentally³ this changes to $D \sim N^{-2}$ and $\eta \sim N^{3.4}$ for N exceeding a critical chain length N_e , the entanglement length. This behavior is usually explained by the reptation model of Edwards⁸ and de Gennes.^{9,10} Physically reptation means that on a length scale larger than $d_T \sim N_e^{1/2}$, the coil dimension of a chain of N_e monomers, the monomers of the chain move predominantly along their own contour. The chain has a Rouse relaxation up to a time $\tau_e \sim N_e^2$. Further relaxation can only occur along the path of a coarse-grained "primitive chain" consisting of monomers containing about N_e bonds. Since this is a one-dimensional diffusion along a random walk path, the chain needs a time $\tau_d \sim N^3/N_e$ to leave the original path or tube. Consequently, one gets¹⁷ $\eta \sim N^3$.

This single-chain picture has been used to develop a rather complete theory of the viscoelastic properties of polymer melts^{2,17} which has proven to be very successful. How-

^{a)} Present address.

ever, there remain several problems, which are not well understood. Experimentally, one clearly finds that $D \sim N^{-2}$ (Refs. 2–6 and references therein), while the viscosity remains at $\eta \sim N^{3.4}$ for a range of N from about $2N_e$ to a value of more than $1000N_e$.¹⁸ This difference between the reptation prediction for the N dependence of η and the experimental observation has been the subject of great controversy. Doi¹⁹ proposed that the difference may be simply a crossover effect and that for very large N , $\eta \sim N^3$. However, as proposed this theory²⁰ probably cannot explain why this crossover occurs for such large values of N . Rubinstein²¹ has recently presented a numerical calculation using the original de Gennes picture of moving defects¹ which shows that the crossover to the asymptotic regime can be delayed considerably, and this may explain why the crossover occurs for such a large value of N . In addition, there have also been a number of alternative attempts to explain the “3.4” power law based on reptation theory.^{22–24} Scher and Schesinger²² point out that the reptation model is a single-chain model and does not necessarily describe all the complicated many-chain effects which contribute to the stress relaxation. Other authors suggest that the experiments do not show a crossover effect but a breakdown of the Edwards–de Gennes picture. Consequently, the entire reptation concept has been called into question and alternative approaches given.^{25–29} However, all of these alternative theories can only treat the interaction between the chains either in a mean-field approximation or develop a memory function formalism. Skolnick *et al.*²⁶ base their approach on the fact that they did not find any evidence for reptation in their simulations of long, lattice polymers.¹⁶ Indeed up until the present work, there has been no simulation or experiment, which can decide which of these models correctly describes the underlying microscopic mechanism. There have been several Monte Carlo^{15,16,30–34} (MC) and one Brownian dynamics simulation¹⁴ which attempted to analyze the behavior of entangled chains. Deutsch³² claimed to see reptation with a specially modified algorithm, in which the mobility of the monomers along the contour was artificially enhanced. These results have been questioned by several authors.^{33,30} Other simulations did not observe any onset of slowing down due to entanglements.^{13,15,16,30} In Ref. 15, reptation theory could only be verified for a mobile chain in a frozen environment. Only very recently a MC simulation of a pearl necklace model³¹ and a reanalysis of lattice data³⁴ showed a slowing down of monomer motion which does not contradict reptation. However, in both cases one cannot identify the mechanism which led to the effects seen. Even the spin-echo experiments of Higgins and Roots³⁵ and Richter *et al.*^{12,36} display contradictory results. Deviations from Rouse behavior are seen; however, they cannot distinguish between the reptation model and some of the alternative formulations.

Even though the present discussion of the confinement and slowing down of the monomer motion has been based on the entanglement concept, there is no precise understanding of what an entanglement actually is. The early reptation papers^{8–10,17} simply introduce it as an adjustable parameter without specifying it completely. There exist several recent attempts to relate entanglements to topological knots.^{37,38}

Other estimates use packing arguments^{39,40} in order to account for the strong dependency on the chemical structure which goes beyond the difference in persistence lengths. Thus it is clear that a better understanding of the microscopic motion of the monomers in a long, entangled polymer melt is still lacking.

Considering the previous discussion on the state of our theoretical understanding of the dynamics of dense melts of entangled polymers, we thought that it would be important to perform a detailed numerical simulation which could hopefully yield an improved insight into these questions and help clear up some of the confusion. To do this we carried out a very extensive molecular-dynamics simulation of a melt of linear chains, which covers the regime from pure Rouse dynamics up to the highly entangled regime. By storing the configurations of all of the chains at regular intervals, we have been able to perform an extensive set of analysis of our data. In this paper, we present our detailed findings for the static and dynamic properties for the range of chain lengths considered. We have structured the paper into units, which are as self-contained as possible. An outline of the material we will discuss is as follows: Sec. II, simulation method and static properties of the polymer melt; Sec. III, motion of monomers; Sec. IV, mode relaxation (generalized Rouse vs reptation); Sec. V, scattering functions; Sec. VI, comparison to experiment and other simulations; Sec. VII, motion of the primitive chain (visualization of reptation); Sec. VIII, summary and conclusions; and in the Appendix, technical details and test of the numerical algorithm. Since the discussion of many of the interesting properties of importance for polymer melts has been extremely brief or nonexistent in the Introduction, each section will contain a more complete description of the relevant theoretical and experimental results.

II. SIMULATION METHOD AND STATIC PROPERTIES OF POLYMER MELTS

A. Method

As we have discussed in Sec. I, computer simulations should be very useful in gaining some much needed insight into the microscopic mechanism of the motion of dense polymers. However, which is the best technique to use? Up to now the method most often chosen has been that of Monte Carlo simulations,^{13,15,16,30–34,41–43} usually but not always on a lattice. For chains on a lattice, in order to obtain a reasonable acceptance rate of the attempted moves and to prevent precursors of the glass transition, the simulations are typically confined to rather low densities. In practice, the largest concentrations that can be used for long chains is about 0.34 for the diamond lattice^{15,16} and 0.5 for the simple cubic lattice.²⁶ There have been a few simulations at higher densities,^{16,30,41} however, it is not clear whether precursors of the glass transition influence these results.⁴³ These lattice MC algorithms are very efficient on sequential, scalar computers but do not work particularly well on modern supercomputers, like the Cray XMP or Cyber 205. One reason is that the algorithms are difficult to vectorize, which is necessary

to obtain the large increases in speed. However, the real problem is that they work only at relatively low to intermediate densities, which means that one is simulating a semidilute solution in the free-draining limit. This means that in order to map the simulations onto a melt, the chains have to be much longer than the screening length, which depends on the monomer density. We will discuss in Sec. VI some of the difficulties in estimating the entanglement length from simulations in which the density is significantly less than that of a melt. For a general discussion of MC simulations for lattice polymers, see Ref. 43; and for simulations of dense polymeric systems, see Ref. 44.

It is clear that in order to gain any significant new insight into the microscopic mechanism of a polymer melt, we need to be able to perform simulations at melt densities. This suggests immediately that one should abandon the lattice and study continuum models. One of the first such studies was by Baumgärtner,³¹ who carried out a MC simulation for a hard-sphere chain at a density of 0.7 (number of monomers per unit volume, bond length $l = 1$) and hard-sphere diameter $h = 0.9l$. These simulations were the first to observe a deviation from Rouse behavior for a completely mobile system. Just as for lattice MC, the technique also does not vectorize very well. However, there appear to be two possible ways out of this problem and they are to use either a Brownian dynamics or molecular-dynamics simulation. While Brownian dynamics simulations have been widely used to study a single dilute polymer,^{45,46} there has been only one attempt which we are aware of to study a many-chain system. Ceperly, Kalos, and Lebowitz¹⁴ studied the early-time behavior for nonentangled polymers and found results in agreement with the Rouse model, but did not study very long chains at high density. Because they were working at moderately high density, they were not able to use the standard Brownian dynamics algorithm for reasonable size time steps ($\Delta t \approx 0.01\tau$, where τ is the unit of time in Lennard-Jones units), and instead had to solve the Smoluchowski equation for the time evolution of the polymer probability density by a MC random walk. The largest chain length they studied was only $N = 63$ at a density of 0.5, and because the method uses a MC sampling, it is very difficult to develop an efficient code suitable for a supercomputer. The third technique, molecular dynamics (MD), does vectorize very well and is very suitable for modern supercomputers. Though MD simulations⁴⁷⁻⁵¹ have been very useful in studying the properties for a wide range of atomic and molecular systems, it has not been widely used in the study of polymers. Most of the previous MD simulations of polymers prior to our work only studied very short chains ($5 \leq N \leq 16$) in a solvent of several hundred monomers.⁵¹ In Ref. 11, we showed that, in fact, MD simulations can be very useful for simulating dense polymer melts.

Here we present the results of simulations for a wide range of chain lengths N from $5 \leq N \leq 400$, using a MD technique recently developed by us.⁵² This method has already proven to be very effective for a many-arm star⁵³ polymer and end-grafted polymer brushes,⁵⁴ where strong density fluctuations occur. Each monomer of the system moves according to the equation of motion,

$$\ddot{\mathbf{r}}_i = \nabla \sum_{j \neq i} U_{ij} - \Gamma \mathbf{r}_i + \mathbf{W}_i(t). \quad (2.1)$$

The interaction potential U_{ij} has two parts. The first U_{ij}^{LJ} is a purely repulsive Lennard-Jones potential which acts between all monomers in the system. Along the sequence of the chain, we add a strong attractive potential^{4,14,52} U_{ij}^{ch} (the parameter we used for this attractive potential differed from earlier simulations¹⁴ so as to avoid any possibility of chains cutting each other. See Ref. 52 and the Appendix for details). Γ is a (small) friction constant which couples the monomers weakly to a heat bath, while $\mathbf{W}_i(t)$ is a Gaussian white-noise source. The strength of the noise is related to Γ via the fluctuation dissipation theorem. The equations were integrated with a time step $\Delta t = 0.006\tau$, where $\tau = \sigma(m/\epsilon)^{1/2}$ is the standard time unit for a Lennard-Jones fluid. We will present most of our results in reduced units in which $\sigma = \epsilon = m = 1$ and the Boltzmann constant $k_B = 1$. As discussed in the Appendix, we set $T = 1.0\epsilon$ and $\Gamma = 0.5\tau^{-1}$. The introduction of a weak coupling to the background is very important not only to keep the temperature at the preset value but also to keep the system stable over the course of the simulation. Because we are interested in the dynamics of a melt in which the relaxation times become very large ($\sim N^3$), we made runs up to $20 \times 10^6 \Delta t$ after equilibration. We found that coupling the system weakly to a heat bath was a physically appealing way to reduce the effect of the numerical errors which accumulate during the course of any long simulation. In the Appendix we show that an alternate technique in which the temperature is rescaled every 100 steps so as to conserve the total energy gives identical results. The overall coupling to a heat bath does, however, lead to a diffusion to the entire system. This diffusion has to be removed when analyzing the motion of the chains. This is done by simply calculating all quantities in the center-of-mass coordinate system of the whole system.

In Table I, we give the number of chains and the length of the chains used in the present study. All of the simulations are carried out at a density of $\rho = 0.85$, which from studies of atomic fluids is relatively high and equals the triple point density for an attractive Lennard-Jones fluid. As we will see below, the height of the pair correlation function at the first peak $g(r)_{\text{max}} \approx 2.7$. However, because the intermonomer interaction is purely repulsive for those monomers which are not connected, we are still far enough away from the glass transition so as not to cause any problems in the interpretation of the results.

B. Equilibration

The first systems ($N \leq 50$) investigated were prepared in a semidilute solution and then slowly compressed to a final density between $0.5 < \rho < 0.90$. We then let the systems equilibrate until the chains moved several chain diameters. From these preliminary studies for small N , we determined that $\rho = 0.85$ was an appropriate density to work at. We wanted to work at high density so the tube diameter would be small, yet we needed to have reasonable relaxation times for chains which would allow us to equilibrate the system in a few million time steps. This turned out to be at $\rho = 0.85$.

TABLE I. Total time of the run T/τ after equilibration, the radius of gyration $\langle R_G^2 \rangle$, mean squared end-to-end distance $\langle R^2 \rangle$, ratio of the moments of inertia $\langle R_{G1}^2 \rangle : \langle R_{G2}^2 \rangle : \langle R_{G3}^2 \rangle$, average pressure \bar{P} , and length of the simulation cell L for the systems studied in the present simulation. Here N is the number of monomers in each chain and M is the number of chains. The monomer density $\rho = 0.85$ for all the runs.

| M/N | T/τ | $\langle R_G^2 \rangle$ | $\frac{\langle R_G^4 \rangle}{\langle R_G^2 \rangle^2}$ | $\langle R^2 \rangle$ | $\frac{\langle R^4 \rangle}{\langle R^2 \rangle^2}$ | $\langle R_{G1}^2 \rangle : \langle R_{G2}^2 \rangle : \langle R_{G3}^2 \rangle$ | \bar{P} | L |
|---------|----------|-------------------------|---|-----------------------|---|--|-----------|-------|
| 50/5 | 3000 | 0.92 | ... | 5.2 | ... | 1.0:4.0:19.2 | 5.55 | 6.65 |
| 25/10 | 7200 | 2.2 | ... | 13.1 | ... | 1.0:3.0:14.3 | 5.20 | 6.65 |
| 30/20 | 12 000 | 5.0 | ... | 29.7 | ... | 1.0:2.9:13.4 | 5.04 | 8.90 |
| 32/25 | 60 000 | 6.3 | 1.16 | 37.8 | 1.53 | 1.0:2.8:12.8 | 4.97 | 9.80 |
| 20/30 | 14 400 | 7.7 | ... | 46.7 | ... | 1.0:2.8:12.9 | 4.99 | 8.90 |
| 16/50 | 42 000 | 13.3 | 1.19 | 82.7 | 1.56 | 1.0:2.7:12.5 | 4.93 | 9.80 |
| 20/75 | 48 000 | 20.1 | 1.21 | 118.3 | 1.63 | 1.0:2.7:12.1 | 4.90 | 12.08 |
| 20/100 | 120 000 | 27.5 | 1.20 | 163.8 | 1.55 | 1.0:2.8:12.3 | 4.90 | 13.30 |
| 20/150 | 90 000 | 42.5 | 1.22 | 263.8 | 1.57 | 1.0:2.8:11.8 | 4.87 | 15.23 |
| 20/200 | 60 000 | 46.1 | 1.79 | 250.7 | 1.53 | 1.0:2.6:9.4 | 4.88 | 16.76 |
| 100/200 | 30 000 | 53.6 | 1.10 | 300.3 | 1.59 | 1.0:2.6:10.7 | 4.84 | 28.66 |

Since all the excluded volume interactions are screened in a melt, one expects that the equilibrium chains should be ideal.¹ That is, the mean-square end-to-end distance of a chain of N monomers should have the form

$$\langle R^2(N) \rangle \equiv \langle (\mathbf{r}_1 - \mathbf{r}_N)^2 \rangle = l^2 l_p^2 (N - 1), \quad (2.2)$$

where \mathbf{r}_1 and \mathbf{r}_N are the coordinates of the chain ends. Here l is the average bond length between two monomers on the chain and l_p is the persistence length [$l_p = (c_\infty)^{1/2}$ in Flory's terminology⁵⁵]. Using Eq. (2.2), we found

$$l = 0.97, \quad l_p = 1.32 \pm 0.02 \quad (2.3)$$

independent of chain length. In the subsequent analysis we use the best estimate from $N = 100$ and 150 for $l_p = 1.34$. While this technique of compressing chains from the semidilute regime was reasonable for beginning our investigations, it was not very useful for longer chains. Because ρ is high, it is simply not possible to place chains randomly on a lattice without strong overlap. An alternative would be to construct an initial state using either stretched chains or some other special nonoverlapping arrangement. However, any such method would need far too much computer time simply to equilibrate. However, knowing l and l_p and that melt chains are ideal, we know a great deal about the global equilibrium structure of our systems. We decided that the most efficient manner was to place M chains of N monomers randomly in a cubic box of volume $V = MN/\rho$. The chains were generated by a simple MC procedure as random walks with a bond length of $l = 0.97$ and with a restriction on backfolding so as to give approximately the correct persistence length. For the present simulation this was achieved by requiring that $|\mathbf{r}_{i-1} - \mathbf{r}_{i+1}| > 1.02$, though this value depends slightly on the chain length for short chains. This provided us with a starting configuration in which the global structure of the chains is very close to the equilibrium structure of the melt but in which many of the monomers overlapped. This method also has proven to be very useful for lattice chains.¹⁵ For 400 , we found for some initial configurations one or two of the chains were stretched by an abnormal amount. When this occurred, we discarded the entire sample and started

over again with a different random sequence. This was necessary because we only had 10 chains. To remove the overlap, so we could begin our numerical simulation, we carried out a standard MD simulation for a few thousand Δt , but replaced the hard-core Lennard-Jones repulsion between monomers that were not nearest neighbors along the chain by a softer potential (because the initial bond length $l = 0.97$, but there was no overlap of attached monomers), which did not diverge at small distance,

$$U(r) = \begin{cases} A(1 + \cos \pi r/2^{1/6} \sigma) & r \leq \sigma \\ 0 & r > \sigma. \end{cases} \quad (2.4)$$

We started the run with $A = 1$ and increased A gradually to about 60 until the overlaps were removed. We also found that by quenching the velocities of all the monomers to zero several times during this initial phase, the monomers moved apart more quickly. This produced a starting state which was very nearly equilibrated and from which we could begin the full simulation. Some care has to be taken, if one wants to use this method for short chains ($N < 30$). There the onset of the excluded volume is strong enough to lead to an overall expansion of the chains. We then equilibrated all of the samples further to up to 5 million steps. In the course of the simulation the chains then moved at least $2\langle R_G^2 \rangle$, the mean-square radius of gyration (except for $N = 200$, which moved about $\langle R_G^2 \rangle$ and $N = 400$ which moved less). We then checked for each system by monitoring $\langle R^2 \rangle$, $\langle R_G^2 \rangle$, etc., that the initial equilibration was sufficient. We also observed that our results for the lengths l and l_p given in Eq. (2.3) were independent of chain length for $5 \leq N \leq 200$. As a final check of the initialization procedure, we produced starting states for $N = 50$ by the two methods and found that both gave the same results for all static and dynamic properties measured.

C. Static properties

Chains in a melt are supposed to be ideal in the sense that they obey random walk statistics. As mentioned above, the mean-squared end-to-end distance $\langle R^2(N) \rangle$ scales as N

as expected. We also measured the mean-squared radius of gyration,

$$\langle R_G^2(N) \rangle = \frac{1}{N} \left\langle \sum_{i=1}^N (\mathbf{r}_i - \mathbf{r}_{cm})^2 \right\rangle \quad (2.5)$$

where $\mathbf{r}_{cm} = \frac{1}{N} \sum_i \mathbf{r}_i$ is the center of mass of the chain.

Figure 1 gives $\langle R^2 \rangle$ and $\langle R_G^2 \rangle$ vs N for $10 \leq N \leq 200$. Clearly both quantities scale with N as expected. The ratio $\langle R^2 \rangle / \langle R_G^2 \rangle = 6$, also as expected for ideal chains. A more precise measure of the Gaussian character of the chains is given by the asphericity and the higher moments of $\langle R^2 \rangle$. In Table I, we give results for $\langle R^4 \rangle / \langle R^2 \rangle^2$. For a random walk, this ratio should be $5/3$. As can be seen, we find a slightly lower value ≈ 1.57 . However, due to the local self-avoidance condition, which is obeyed for these chains, one can only expect to find perfect Gaussian statistics in the limit $N \rightarrow \infty$. Another measure of whether the dimensions of the chains can be regarded as ideal is the asphericity of the coils. In the case of an ideal random walk, the ratio of the eigenvalues of the inertia tensor are $1:2.5:11.8$.^{56,57} The sum of the three eigenvalues is of course just $\langle R_G^2 \rangle$. The data in Table I show that for the longer chains this limit is approximately satisfied. Only the data for the small $N = 200$ system show a clear deviation. Because the chains are Gaussian, as N increases, the number of chains M must also increase, roughly as $N^{1/2}$ to ensure that the chains do not interact with themselves via the periodic boundary conditions. From the chain dimensions given in Table I, it is clear that except for $N = 400$, there are a sufficient number of chains so that the effect of the periodic boundary conditions will not play a significant role in the dynamics. If we want to study the long-time behavior for $N = 400$, we would need at least 40 chains, which is beyond the scope of the present simulation. The real bottleneck, however, for $N = 400$ is the very slow relaxation. However, as we demonstrate in Sec. VI, the $N = 400$ sample is very helpful in visualization of the motion of the primitive

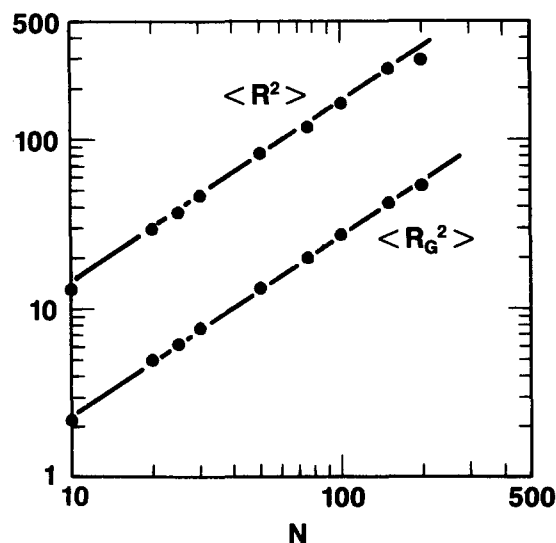


FIG. 1. Mean square end-to-end distance $\langle R^2(N) \rangle$ and radius of gyration $\langle R_G^2(N) \rangle$ vs N for $10 \leq N \leq 200$. The lines give the expected slope of 1.

chain. We did not use the data for $N = 400$ for determining any static or dynamic quantities. The reader may also notice from Table I that for $N = 200$ we ran systems of size 20 and 100. The system with $M = 20$ contains just about the minimum number of chains which we feel are necessary to obtain reliable data for the dynamics at long time. Except for the fact that $\langle R^2 \rangle$ and $\langle R_G^2 \rangle$ were slightly too small for the $M = 20$ system compared to the $M = 100$ system and as expected from smaller N , all of the dynamic results for both sizes are the same within the statistical errors.

So far, we have only presented results for the global properties of the chains, which indicate an overall equilibrium structure. However, most of the analysis will be confined to intermediate times and length scales smaller than $\langle R^2 \rangle^{1/2}$. Thus it is important that we check the internal structure of the chains as well. One way this can be done is to determine the coherent structure function $S(q)$ of an individual chain,

$$S(q) = \frac{1}{N} \left\langle \left| \sum_{i=1}^N \exp(i\mathbf{q} \cdot \mathbf{r}_i) \right|^2 \right\rangle. \quad (2.6)$$

$S(q)$ was determined by averaging over 20 randomly chosen \mathbf{q} vectors every 60τ for $N \geq 100$ and every 6τ for $N < 100$. For $2\pi/\langle R^2 \rangle^{1/2} < q < 2\pi/l_p$ we expect the fractal scattering of $S(q) \sim q^{-1/\nu} = q^{-2}$ ($\nu = 1/2$) independent of chain length. Figure 2 shows that this is fulfilled by the data. From a plot of $q^2 S(q)$ (not shown), one can see a small overshoot for the low q limit. It is not clear to us whether this is always the case for chains in the melt or just a result of the sampling statistics. For single chains one knows that due to the fluctuations of the ends, damped oscillations can be found in the plateau regime of $q^{1/\nu} S(q)$.⁵⁸ Disregarding this possibility, we estimate that the best fit to the exponent $\nu = 0.48$, which is very close to the expected value of $1/2$.

Another check of the internal structure of the chains is to study the Rouse modes of the chain. For a finite discrete monomer chain these are given by^{59,60}

$$\mathbf{X}_p(t) = \frac{1}{N} \left[\sum_{i=1}^N \mathbf{r}_i(t) \cos \frac{p\pi(i-1)}{N-1} \right] - \frac{1}{2N} [\mathbf{r}_1(t) + \mathbf{r}_N(t)]. \quad (2.7)$$

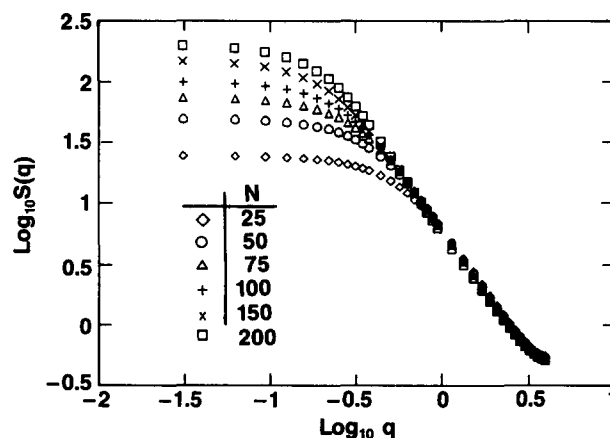


FIG. 2. $S(q)$ vs q for six values of N .

For ideal chains these modes are eigenmodes. Within the fluctuations of the data we find $\langle \mathbf{X}_p(t) \cdot \mathbf{X}_{p'}(t) \rangle = 0$ for $p \neq p'$. One expects² that the amplitudes obey the scaling relation

$$\langle \mathbf{X}_p(t) \cdot \mathbf{X}_{p'}(t) \rangle = \frac{1}{2\pi^2} \langle R^2(N) \rangle / p^2 \propto N/p^2. \quad (2.8)$$

Figure 3 gives $\langle X_p^2 \rangle$ vs p for $10 \leq N \leq 200$. Equation (2.8) describes the behavior very well except for the first mode $p = 1$ (which seems to be strongly effected by the chain ends). The agreement with Eq. (2.8) was valid for all chains studied and also is in accordance with the effects seen for $S(q)$. Taking all of the information presented, we believe that all of the samples we used to investigate the dynamics have been well equilibrated.

Since all of the runs were made at constant density, the relative effect of the free ends decreases with increasing chain length. One way this shows up very clearly is in the average pressure \bar{P} . As seen in Table I, \bar{P} decreases with increasing N . This decrease is rapid for $N < 25$ but much smaller for $N \geq 30$, indicating that for large N the end effects on the pressure are negligible. A similar behavior also is seen in the glass transition temperature which varies strongly with N for short chains, but saturates for large N .⁶¹ This already gives us a first hint that the chain lengths considered are sufficient in order to cover the crossover regime from the nonentangled to the entangled state.

The internal structure of such a complex fluid is also of interest.⁶² This is particularly true for the formation of networks, such as gels and rubber, where one needs to know about the details of the local structure.⁶³⁻⁶⁵ Figure 4 gives the radial distribution function of all the monomers in the system. Besides the strong nearest-neighbor correlation due to the connectivity of the chain, the results are not unlike a simple, atomic fluid. More interesting is the intrachain distribution function shown in Fig. 4(b), which describes the probability for monomers of the same chain to meet each other. Figure 5 gives the probability that a monomer a chem-

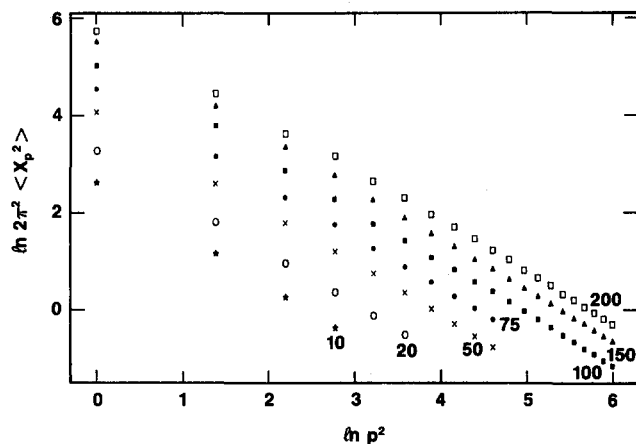


FIG. 3. Amplitude of the Rouse modes $\langle X_p(1) \cdot X_p(0) \rangle \cdot 2\pi^2$ vs N/p^2 for several values of p and N . The results are normalized such that the data for $p = 1$ give $\langle R^2 \rangle$.

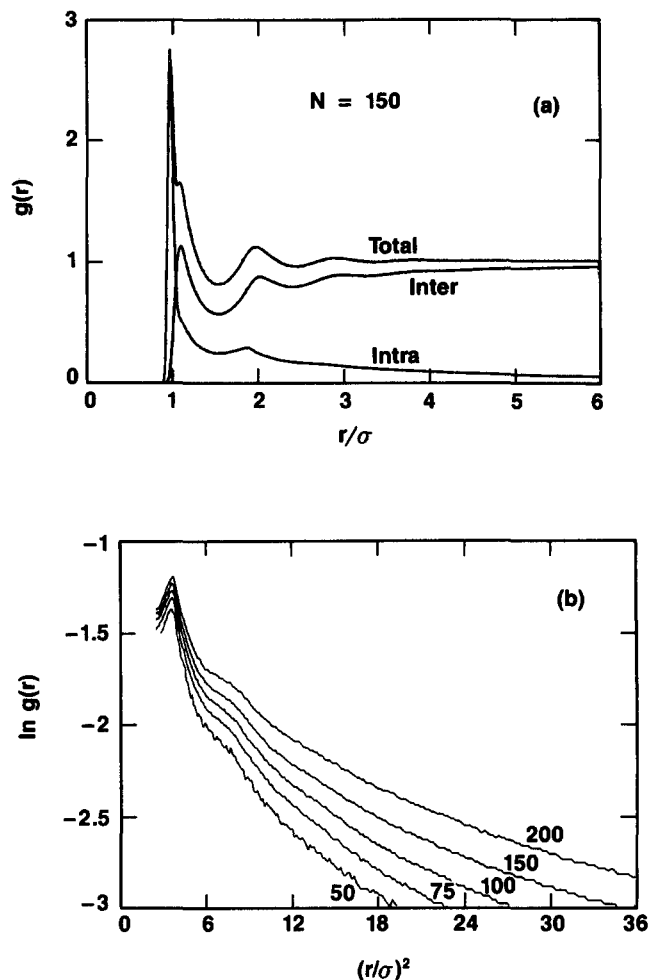


FIG. 4. (a) Pair correlation function $g(r)$ vs r for $N = 150$. The upper curve is for all monomers in the system; the middle curve is the interchain correlation function in which monomers i, j are on different chains; and the lower curve is the intrachain correlation in which i, j are on the same chain. The upper curve is simply the sum of the other two curves. (b) Intrachain correlation function $g(r)$ vs r^2 for five values of N .

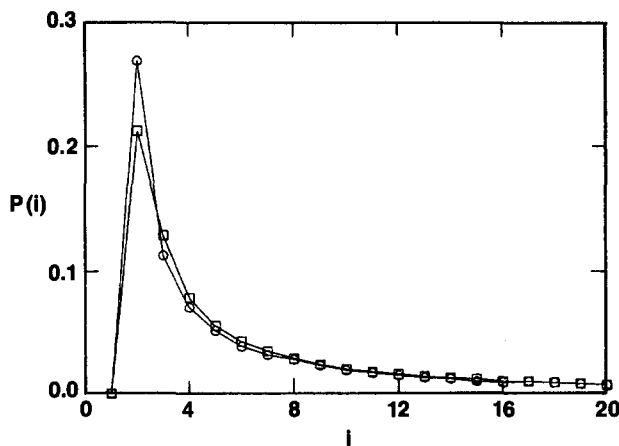


FIG. 5. Probability that a monomer which is a chemical distance j from the end of the chain is within a distance r from that end monomer for $N = 150$. The monomer at $j = 1$ which is connected to the end has been excluded. The squares are for $r = 2.0$ and circles for $r = 1.5$.

ical distance j from the chain end is physically near the end. This quantity would thus describe the length distribution of self-loops for a network in which ends are randomly cross-linked to another monomer of the melt. Note that in the present case $\sim 14\%$ of the chain ends would form loops, if we consider random crosslinking of the ends with a monomer nearby within a sphere of radius l_p .

III. MOTION OF MONOMERS

This section contains a detailed discussion of the motion of the individual monomers. In order to provide this, we first present some background concerning the various theoretical approaches, which have been discussed in the literature. However, we will restrict our discussion to quantities which can be investigated directly by simulation.

A. Theoretical concepts

The motion of a single monomer is governed by the connectivity of the chain and the interaction of the monomer with its surroundings. In the simplest model, one can think that for such a situation all the complicated interactions are absorbed into a monomeric friction and a coupling to a heat bath. For this model, the Rouse model,^{7,2} the motion of each monomer is described by a Langevin equation

$$\dot{\mathbf{r}}_i = \frac{-1}{\zeta} \nabla U(\{\mathbf{r}_i\}) + \mathbf{f}_i(t), \quad (3.1)$$

where \mathbf{r}_i denotes the position of monomer i , ζ is the friction coefficient with the viscous background, U is the potential which keeps the chains connected, and $\mathbf{f}_i(t)$ is a random force. The strength of $\mathbf{f}_i(t)$ and ζ are related by the fluctuation dissipation theorem. Note that this model does not contain any specific interaction between monomers except that due to the chain connectivity. The Rouse model can be solved and gives for the diffusion coefficient D and viscosity η ,

$$D = \frac{kT}{N\zeta}, \quad \eta \propto N. \quad (3.2)$$

The largest relaxation time of the chain is then given by²

$$\tau_N = \zeta N \langle R^2(N) \rangle / 3\pi^2 kT. \quad (3.3)$$

The mean-square displacement of a monomer $g_1(t)$

$$g_1(t) = \frac{1}{N} \sum_{i=1}^N \langle [\mathbf{r}_i(t) - \mathbf{r}_i(0)]^2 \rangle \quad (3.4)$$

with time is governed by the fact that as time increases an increasing number of monomers have to be carried along. Using the fact that the chain structure is that of a random walk, it is easy to show that

$$g_1(t) \propto \begin{cases} t^1, & t < \tau_0, \quad g_1(t) < l^2 \\ t^{1/2}, & \tau_0 < t < \tau_N, \quad g_1(t) < \langle R^2 \rangle \\ t^1, & t > \tau_N, \quad g_1(t) > \langle R^2 \rangle. \end{cases} \quad (3.5)$$

It turns out experimentally that this extremely simple model provides an excellent description of polymer dynamics, provided that the chains are short enough. Measurements³⁻⁶ of η as well as NMR (Ref. 66) and neutron scattering experi-

ments^{12,35,36} which directly probe the motion via spin-echo techniques are in agreement with Eq. (3.2). However, simulations have been somewhat difficult to interpret in this respect. Up to now, simulations of dense systems have either used Monte Carlo or Brownian dynamics methods. For both of these cases the Rouse model is inherently built in. It is difficult to decide how much of the observed behavior can be directly attributed to the interactions and how much to the algorithm (see the Appendix and Sec. VI).

For the MD algorithm we use in the present investigation the situation is clearer. The value of Γ chosen ($\Gamma = 0.5\tau^{-1}$) is so small that the typical $t^{1/2}$ behavior in Eq. (3.5) for the unperturbed chain sets in at a distance of 2-3 bond lengths.⁵² Thus if we observe this behavior for shorter times and distances, it reflects the interactions of the individual beads.

For chains which significantly exceed the critical entanglement length N_e , the motion is slowed down drastically. Experimentally, one finds

$$D \propto N^{-2}, \quad \eta \propto N^{3.4}. \quad (3.6)$$

The reptation concept gives a very nice physical picture for this slowing down. The idea is that the chain moves on a coarse-grained scale mainly along its own contour. The reason for this is that the topology of the surrounding suppresses the motion transverse to its own contour. For short time scales the motion of the monomers cannot be distinguished from that of the Rouse model. When the distance a monomer moves exceeds a critical size, namely the so-called tube diameter d_T , one only has Rouse relaxation along this coarse-grained random walk structure. The typical time for the onset of this constraint motion is given by

$$\tau_e \sim N_e^2. \quad (3.7)$$

Since one has Rouse-like behavior along a random walk path,^{9,10} the $t^{1/2}$ power law for $g_1(t)$ becomes a $t^{1/4}$ power law. After the chain along this path is relaxed ($t > \tau_N \propto N^2$), it has only moved a distance of the order of the square root of the contour length of the tube. Then one should observe an overall diffusion along the tube yielding a second $t^{1/2}$ regime for the motion in space. Finally, after a time $\tau_d \propto N^3/N_e$, the so-called disentanglement time, the overall diffusion of the polymer chain in space is observed. Thus we expect the following general power-law sequence (Fig. 6) for the mean-square displacement in space, $g_1(t)$:

$$g_1(t) \sim \begin{cases} t^1, & t < \tau_0 \\ t^{1/2}, & t < \tau_e \sim N_e^2 \\ t^{1/4}, & t < \tau_N \sim N^2 \\ t^{1/2}, & t < \tau_d \sim N^3/N_e \\ t^1, & t > \tau_d \end{cases} \quad (3.8)$$

Similar behavior is expected for the mean-square displacement in the center of gravity of the chain itself $g_2(t)$,

$$g_2(t) = \frac{1}{N} \sum_{i=1}^N \langle [\mathbf{r}_i(t) - \mathbf{r}_i(0) - \mathbf{r}_{c.m.}(t) + \mathbf{r}_{c.m.}(0)]^2 \rangle, \quad (3.9a)$$

and the motion of the center of mass $g_3(t)$,

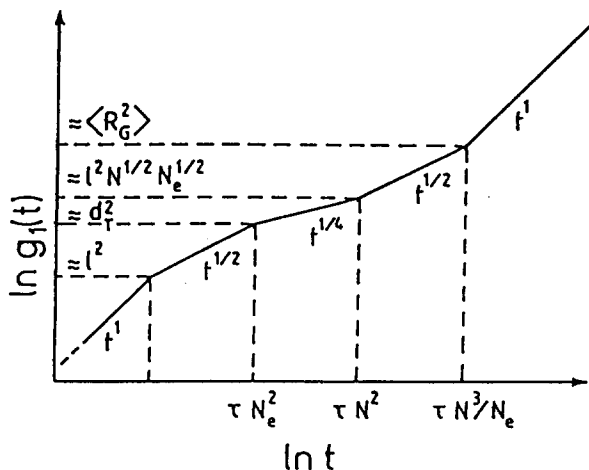


FIG. 6. Schematic plot of the mean-square displacements for the reptation model.

$$g_3(t) = \langle [r_{c.m.}(t) - r_{c.m.}(0)]^2 \rangle. \quad (3.9b)$$

The reptation model predicts that $g_2(t)$ and $g_3(t)$ have the form

$$g_2(t) \sim \begin{cases} t^1, & t < \tau_0 \\ t^{1/2}, & t < \tau_e \\ t^{1/4}, & t < \tau_N \\ t^0, & t > \tau_N \end{cases} \quad (3.10a)$$

$$g_3(t) \sim \begin{cases} t^1, & t < \tau_e \\ t^{1/2}, & t < \tau_N \\ t^1, & t > \tau_N. \end{cases} \quad (3.10b)$$

For several years it has been the main concern of many simulation studies as well as experimental investigations using neutron spin echo to search for these power laws in order to confirm or reject the basic reptation picture. However, there remain many unanswered questions. The reptation idea is a conceptually simple single-chain approach. The largest relaxation time $\tau_d \propto N^3$ contradicts the measured viscosity which scales $N^{3.4}$. Also, the idea of rigid topological obstacles forming the entanglements is still under discussion. It is clear that the background moves as well and this leads to a release and reconstruction of constraints.⁶⁷⁻⁷¹ However, it is not yet clear whether an entanglement is a consequence of the chain topology or just a result of a diverging mass which has to be moved, as, e.g., a packing criterion would suggest.³⁷⁻⁴⁰

Consequently, several other attempts have been made to describe the motion of the chain. Hess²⁷ used a projection operator formalism in order to account for the topological constraints. He solved his model self-consistently within the framework of the Rouse model. By his approach a more microscopic foundation for a reptation-like ansatz is given under certain circumstances. His theory especially points out the importance of constraint release. His ansatz self-consistently introduces an explicitly time-dependent friction coefficient. In the limit of small constraint release, the characteristics of the reptation model, e.g., in the mode spectrum, are recovered. Ronca²⁵ used a memory-function approach.

This in some sense is similar to Hess. However, here the time dependence of the friction coefficient comes from the *ad hoc* assumption of the form of the memory function. Kavassalis and Noolandi²⁹ employ the so-called generalized Rouse model (GRM). Skolnik and Yaris²⁶ simplified Hess' treatment in order to account for different intermediate power laws they observed for the motion of the chain. There the explicit time dependence of the self-consistent friction coefficient was abandoned. Details of these different models will show up more clearly in the discussion of the Rouse modes (Sec. IV). However, the mere investigation of the motion of the monomers will give significant insight as well. It will also give us a clear picture of the parameter space we can cover. But it will not really be sufficient to decide which physical ansatz is the most appropriate. For this we need additional information, which we will discuss in the following sections.

B. Analysis of chain motion

For the analysis of the motion of the chains we ran the systems up to $20 \times 10^6 \Delta t$ ($t_{\max} = 120\,000\tau$) as seen from Table I. Averaging was performed up to at most a third of this total time. The averaging of motion then effectively is done over at least 60 independent chains for the longest chains at the longest times except for 100/200. Assuming $3d$ random walk statistics for the motion of the chains, the statistical error in our results is of the order of 10% in the worst case. However, it should be noted that the error bars decrease progressively with decreasing time intervals. The estimate of the error given above is supported by the comparison of statistically independent systems, such as those with different chain lengths. For all investigations of the monomer motion the overall system diffusion has to be taken out. For details see the Appendix.

1. Diffusion

In order to get an impression of how far into the entangled regime our chains reach, consider first the mean-squared displacement of the center of mass $g_3(t)$ (Fig. 7). For long time one gets $g_3(t) = 6Dt$, which is how we deter-

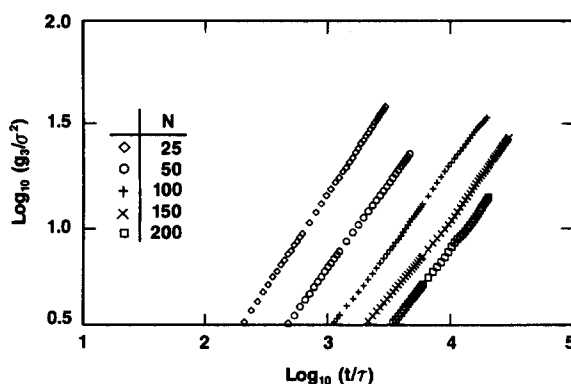


FIG. 7. Center-of-mass diffusion $g_3(t)$ vs t/τ for five values of N . Data from $N = 200$ are for the $M = 20$ system.

mine D by extrapolation. We include for $N = 200$ extrapolated data of the large system, although it did not run into the diffusion limit. The error bar in Table II gives an estimate of the uncertainty in extrapolation. Also for $N = 200$, the system of only 20 chains would be too small to determine D properly. As one can see from the data there is already a significant short-time regime showing an effective slope less than 1 for $N = 100$. For $N \gg 100$ the effective minimal slope is about 0.70. The onset of this slowing down is at about $t \approx 200\tau$. From reptation one expects a slope of $t^{1/2}$ for the intermediate regime. However, it is known even for chains in a frozen environment where the chains clearly reptate, that this intermediate power law of $1/2$ is difficult to obtain.¹⁵ Somewhat more insight can be gained from Fig. 8 where ND is plotted vs N . The figure clearly shows that the chain lengths considered cover the crossover regime. From Figs. 7 and 8 we can obtain our first estimate of N_e . It is known that the crossover in D occurs at about $N_c = 2N_e$. For this intermediate regime several expressions for N_e have been given. Graessley,⁶ e.g., used

$$D(N) = \frac{4}{15} D_{\text{Rouse}}(N) N_e/N, \quad (3.11)$$

where D_{Rouse} is the corresponding diffusion constant in the Rouse model, Eq. (3.2). Using this yields a value for N_e of 120 monomers. Other equations differ considerably. Hess,²⁷ e.g., finds (with $N_e = 0.5 N_c$ in his notation) $D/D_{\text{Rouse}} = N_e/(N_e + N)$ yielding $N_e \lesssim 50$. However, a closer look at the data for $g_3(t)$ in Fig. 7 shows that the estimate from Eq. (3.11) is clearly too high. Following both the Rouse and reptation models, one expects for the motion of the center of mass,

$$g_3(t) = 6D_{\text{Rouse}}(N)t, \quad t < \tau_e. \quad (3.12)$$

Using this and comparing it to the onset of the slower than linear t dependency observed for g_3 , we expect N_e to be considerably smaller than 120.

TABLE II. Diffusion constants and bead frictions from the mode analysis for $N/p < N_e$.

| N | $6D(\sigma^2/\tau)^a \times 10^3$ | $\xi_\mu(\tau^{-1})^b$ |
|------------------|-----------------------------------|------------------------|
| 200 ^c | 0.35 | 24 ± 3 |
| 150 | 0.6 ± 0.14 | 24 |
| 100 | 1.65 ± 0.25 | 24 |
| 75 | 2.73 | 26 |
| 50 | 4.80 ± 0.40 | 20.5 |
| 30 | 11.0 | 19 |
| 25 | 13.2 | ... |
| 20 | 18.7 ± 1.0 | 18 |
| 10 | 38 | 17 ± 2 |
| 5 | 80 | 15 |

^a Typical error bars are given. If not shown they are similar to the neighbor data.

^b The error bars give the typical accuracy in the fluctuations of the high p modes.

^c The upper limit is 0.40. We expect the lower limit to be at a similar deviation; however, we cannot give a reliable number from the simulation.

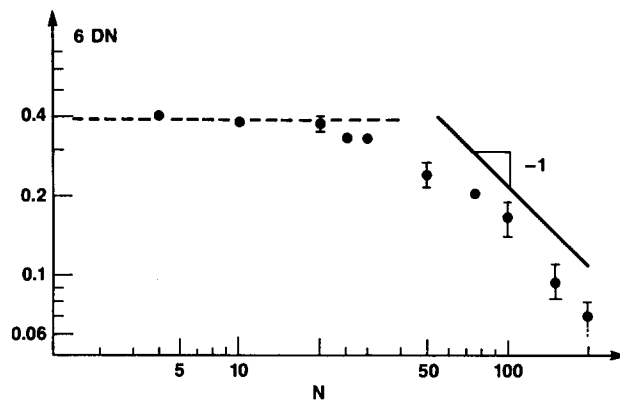


FIG. 8. Diffusion constant $6DN$ vs N . D was obtained from the long-time behavior of $g_3(t)$, given in Fig. 6. For $N = 200$ only an upper limit is given.

2. Monomer motion

The behavior of the diffusion constant showed that the systems considered are in the crossover regime. Thus in order to observe the influence of the (topological) constraints introduced by the surrounding, we first confine ourselves to the innermost monomers,

$$g_1^i(t) = \frac{1}{3} \sum_{i=N/2-2}^{N/2+2} \langle [\mathbf{r}_i(t) - \mathbf{r}_i(0)]^2 \rangle, \quad (3.13)$$

$$g_2^i = \frac{1}{5} \sum_{i=N/2-2}^{N/2+2} \langle \{ [\mathbf{r}_i(t) - \mathbf{r}_{i.c.m.}(t)] - [\mathbf{r}_i(0) - \mathbf{r}_{i.c.m.}(0)] \}^2 \rangle,$$

where $\mathbf{r}_{i.c.m.}(t)$ is the center-of-mass chain i . Figure 9 shows our results. Note that for short times only a few points are plotted; however, as shown in Ref. 11, the data for all systems fall exactly on top of each other. The results in Fig. 9 demonstrate for short times and lengths excellent agreement with the expected Rouse behavior. For the background frictional coefficient $\Gamma = 0.5\tau^{-1}$ used in these runs, the Rouse-like behavior for a free self-avoiding walk with the same parameters as used here only starts for $g_1(t) \approx 20$ and $t \approx 20$ – 30τ . Thus the apparent early $t^{1/2}$ regime is a consequence of the bead–bead interaction and not of the algorithm. It is also important to note that the inner monomers for short times

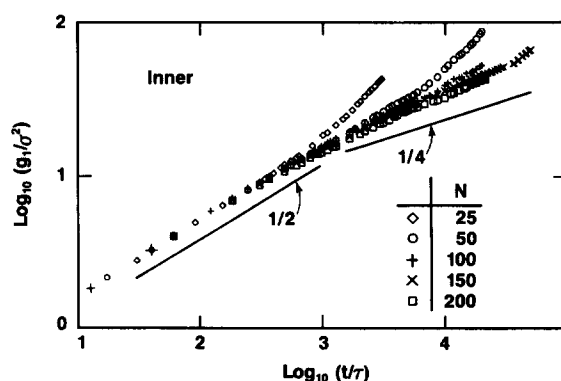


FIG. 9. Mean-square displacement $g_1(t)$ vs t/τ averaged over the inner five monomers for five values of N .

hardly know what the total length of the chain is that they are connected to. With increasing time for $N = 25$, we observe a direct crossover from this $t^{1/2}$ regime to free diffusion. However, as the chain length increases, we observe a definite decrease of the slope in the intermediate regime. The onset of this slowing down occurs at the same time and amplitude for all systems for $N \gg 100$. Again, this is an important check on the validity of our simulation. Reptation theory would require a $t^{1/4}$ power-law regime, while our data give a slope of about 0.28 ± 0.03 . Thus within the error bars the expectations of the reptation theory for $g_1(t)$ are confirmed. The onset of the $t^{1/4}$ regime can be identified as τ_e , giving $\tau_e \approx 1800\tau$ with $g_1(\tau_e) \approx 20\sigma^2$. Assuming that τ_e is the relaxation time of a Rouse chain of N_e monomers, one gets $g_1(\tau_e) \sim g_2(\tau_e) = 2\langle R_G^2(N_e) \rangle$. With $l_p = 1.34$ and $l = 0.97$, one gets $N_e \approx 35$. It assumes, that at τ_e the subchains of length N_e are relaxed. Taking this into the motion function g_2 yields the above estimate. g_1 certainly is larger, however, since we do not have chain ends which partially compensate for this. Thus we think, that this estimate is a reasonable first guess. This estimate of N_e is independent of the chain length and thus differs from the estimates of N_e which depend on N , as given for instance by Kavassalis and Noolandi.⁴⁰ For these theories, the constraint release mechanism, namely the deformation of the tube due to the motion of the ends, plays the dominant role in determining the effective entanglement length. The above results show that for the innermost monomers the initial slowing down of the motion is not affected that strongly by constraint release. It may still be possible that even with increasing chain length we do not find $t^{1/4}$ exactly as a consequence of constraint release. However, in order to prove such a speculation much longer chains are needed. Since our estimate of N_e is independent of chain length, we can conclude that this is probably also a good estimate of the asymptotic value for N_e . In order to prove reptation from an analysis of the mean-square displacement, one also would need to identify the second $t^{1/2}$ regime. However, even if the chains would strictly move in a tube of diameter d_T this regime would be difficult to obtain unambiguously for the present chain lengths. As earlier investigations of a chain in a straight tube⁴² showed, the plateau value/time for $g_2(t)$ is a strongly varying function of the position of the monomer along the chain. Even in this case there are problems with the predictions of the reptation model itself. Consequences of this for the scattering function $S(k,t)$ will be discussed in Sec. V.

Experiments typically see the entangled behavior only for chains containing many N_e monomers. In light of the above discussion one would expect strong influence of the positions of the monomers along the chain. To illustrate this, we present in Fig. 10 results for $g_1(t)$ and $g_2(t)$ averaged over all monomers of the chain on their dynamics. These figures hardly show any deviation from the Rouse-like behavior. For $N = 150$ the apparent minimal slope in $g_1(t)$ is about 0.45, which is far from the predicted $1/4$. To illustrate this in more detail, Fig. 11 presents our results for $g_1(t)$ and $g_2(t)$ for averaged over monomers from different positions along the chain for $N = 150$. What is striking is the extremely enhanced mobility of the outer beads. Their fast motion is

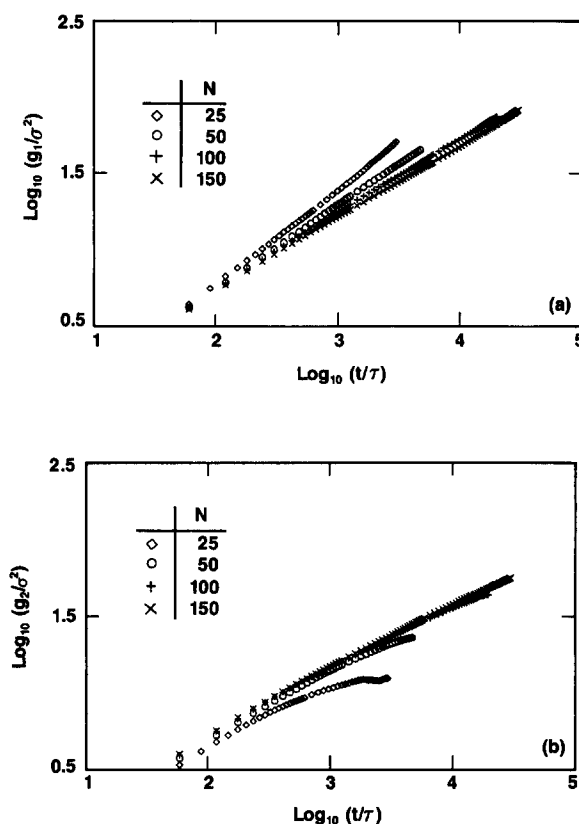


FIG. 10. Mean-square displacements $g_1(t)$ (a) and $g_2(t)$ (b) vs t/τ averaged over all the monomers on the chain.

actually slowed down by the much less mobile center monomers. When analyzing Fig. 11 one sees again that one typically has to consider only monomers which are N_e to $1.5N_e$ inward in order to observe the "position-independent onset" of the slowing down. Experimentally, it is known that the monomeric friction coefficient ζ increases with chain length. It changes from short-chain melts to highly entangled melts by about a factor of 1.5.^{72,73} Figure 11 gives a direct explanation for this phenomena. Short chains with the order of N_e monomers consist of essentially only "outer" monomers, while very long chains only contain "inner" monomers. Again as a consistency check and to support the above ideas, we show that the mobility change coming from the chain ends is independent of chain length (Fig. 12). It should already be mentioned here that neutron scattering experiments^{12,35,36} up to now have only been performed with homopolymers. Figures 11 and 12 strongly suggest the use of triblock chains in order to reduce the influence of the ends. (See Note added.)

IV. MODE RELAXATION: GENERALIZED ROUSE vs REPTATION

The preceding section mainly discussed quantities which are not directly accessible experimentally. In order to give more definitive answers about the validity of the various theoretical approaches and to also give a more coherent description of the physical situation we have analyzed the normal modes of our chains. The dynamical behavior of the normal modes is experimentally accessible in a variety of

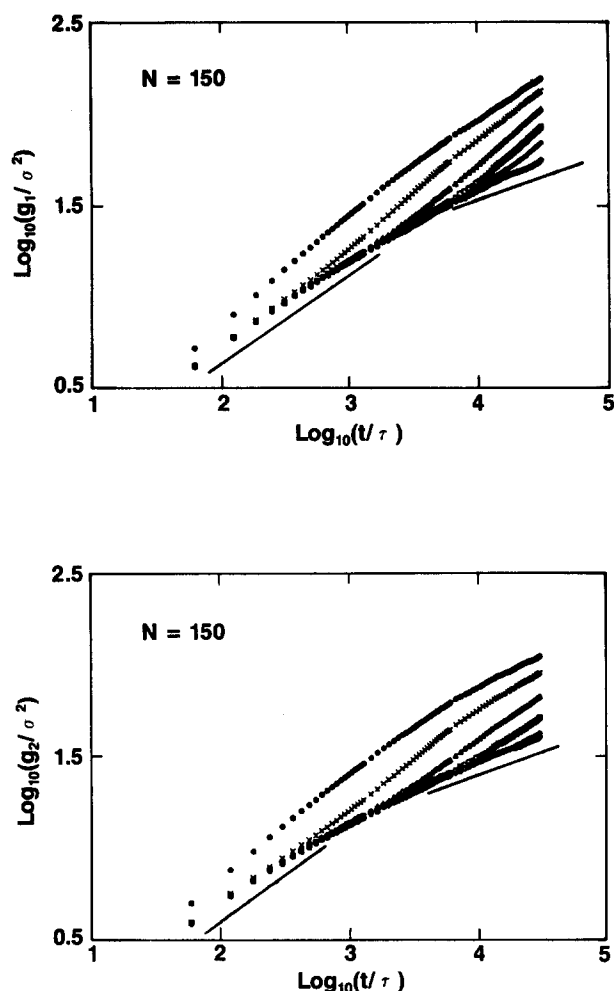


FIG. 11. Mean-square displacements $g_1(t)$ (a) and $g_2(t)$ (b) vs t/τ averaged over different segments of the chain. In each case, the upper curve is averaged over the outer five monomers, the next curve is averaged over monomers 8–12, the third curve from 18–22, and so on. The lowest curve is averaged over the center five monomers.

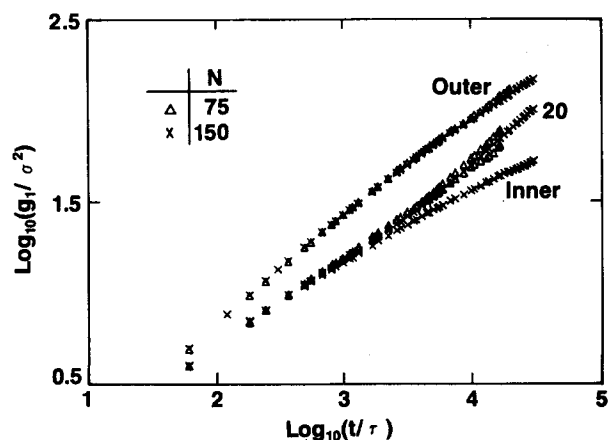


FIG. 12. Mean-square displacement $g_1(t)$ vs t/τ averaged over different segments of the chain for $N = 75$ and 150 . The upper curves are averaged over the outer five monomers, the center curves over monomers 18–22, and the lower two over the inner five monomers.

relaxation experiments (e.g., dielectric relaxation and viscoelastic relaxation). Also, knowledge of the mode spectrum allows one to give a definitive answer as to whether the original reptation ansatz, one of its more microscopic formulations, or one of the simplified generalized Rouse models reproduce the appropriate physics. As discussed in Ref. 11, the Rouse modes of the chains indicate a length-dependent transition from typical short-chain dynamics to a slower long-chain dynamics. Here we present a more detailed analysis of an extended set of data.

In the context of the analysis of the static structure of the chains, the Rouse modes $X_p(t)$ as defined by Eq. (2.7) were shown to be eigenmodes of the chains. Following the Rouse model for the relaxation function of the modes, one gets

$$g_p(t) = \frac{\langle X_p(t) \cdot X_p(0) \rangle}{\langle X_p(0) \cdot X_p(0) \rangle} = \exp(-t/\tau_p) \quad (4.1)$$

with

$$\tau_p = \frac{\zeta_\mu \langle R^2 \rangle N}{3\pi^2 k_B T p^2} = \frac{\zeta_\mu l^2 l_p^2 N^2}{3\pi^2 k_B T p^2}, \quad (4.2)$$

where p is the index of the mode [Eq. (2.7)] and ζ_μ is the monomeric friction coefficient. As seen from the second equation in (4.2), the relaxation time of the p th mode is just the longest relaxation time of a chain of N/p monomers. This reflects the fact that the standard formulations of the Rouse model use periodic boundary (no end effects) conditions and take no additional interaction into account besides the connectivity of the chain. It is one of the least understood phenomena in polymer science why such a rather crude model works so well in describing short-chain melts.

In Fig. 13, we present four examples which are typical of our results for $g_p(t)$. They display a clear single-exponential decay for the short chains [Figs. 13(a) and 13(b)]. For $N > 100$, however, there seems to be two different time scales for the long-wavelength modes. From an analysis of the relaxation functions one gets the relaxation times given in Table II. A clearer picture can, however, be obtained by considering the scaling of the modes with N and p .

A. Rouse relaxation on short (sub) chains

Following Eq. (4.2), one would expect that the relaxation plots for the different modes should collapse onto a single curve if time t is scaled by $(p/N)^2$. This would be a direct verification of the Rouse behavior for short chains. For long, entangled chains, one would also expect standard Rouse behavior for segments of the chain for which $N/p < N_e$, since these modes relax in a time $\tau_p < \tau_e$. In Fig. 14 we give typical examples of such scaled plots. Common to all curves is a fast short initial drop. After that in the initial regime for all the short chains $N \lesssim N_e$ the data nicely collapse onto a single curve, while for the lower modes (small p) of the longer chains the data do not scale as well as the $N = 100$ data [Fig. 14(c)] show. The data suggest, in agreement with the calculation of Hess,²⁷ that for these time and length scales the system almost perfectly reproduces the Rouse model as long as $N \lesssim N_e$. This would also mean that all the data for the different N should follow one unique curve. This is not the case. The slope decreases with increasing chain length, indi-

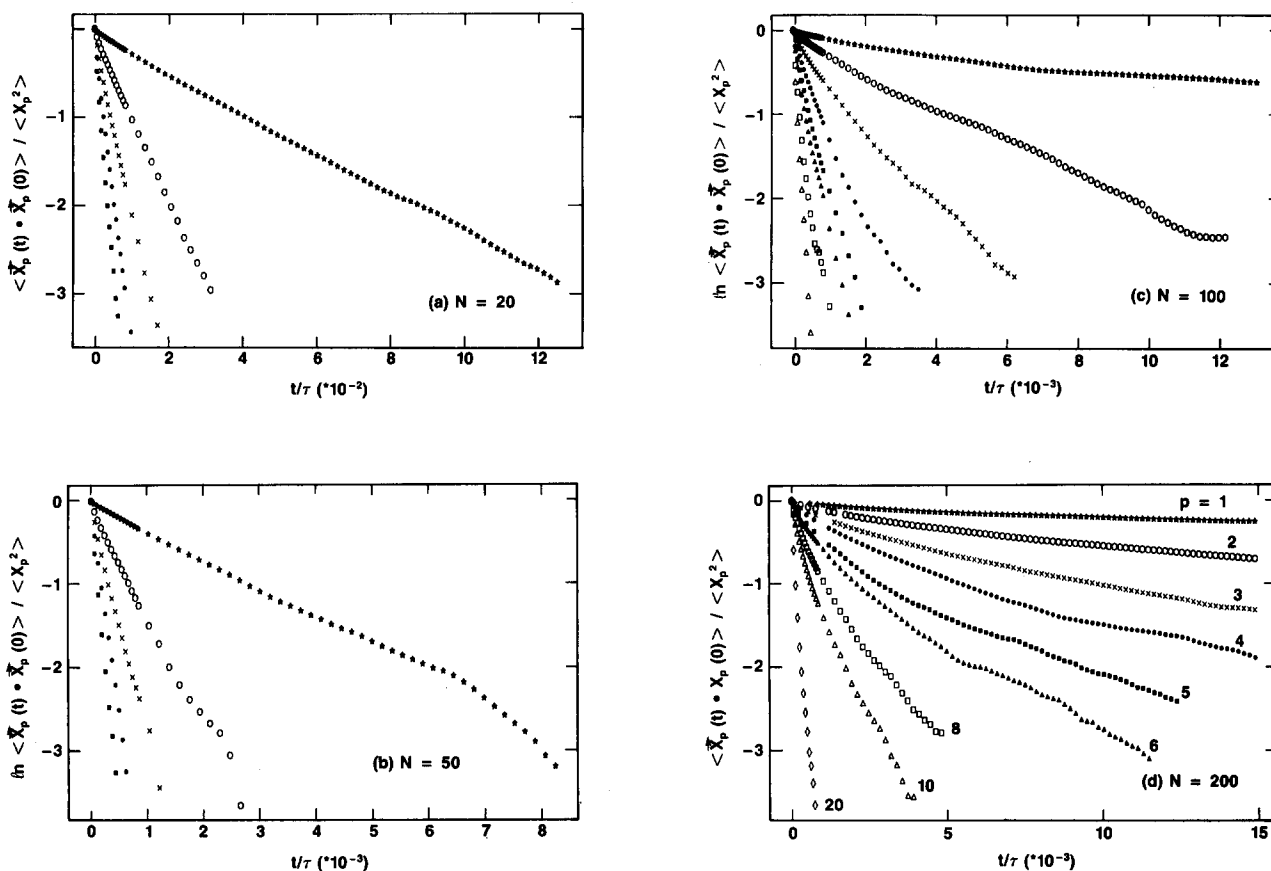


FIG. 13. Typical relaxation plots of the logarithm of the mode autocorrelation function $g_p(t)$ for $N = 20$ (a), 50 (b), 100 (c), 200 ($M = 100$) (d). The correspondence between mode index p and symbol is indicated in (d).

ating a change in the effective monomeric friction coefficient. This picture does not change if we confine the analysis to a short internal subchain. The only difference is the initial drop, indicating the effect of the free ends. It is known from diffusion experiments and viscoelasticity that the monomeric friction coefficient calculated from samples of short chains differs from that determined from highly entangled systems by up to a factor of 2. This is sometimes related to the free ends of the chain, which as seen in Sec. III are much more mobile than the center of the chain. According to this conjecture, the apparent monomeric friction coefficient should increase around $N \gtrsim N_e$. Since we have analyzed the decay of the individual normal modes, we can check this directly. Figure 15 shows the results. For $N \gtrsim 75$, we see that the normalized relaxation time $\tau_p (p/N)^2$ seems to reach a plateau around $1.45\text{--}1.5\tau$, while for shorter chains the value of $\tau_p (p/N)^2$ decays and extrapolates to a value about 1.0τ . Following Eq. (4.2), we find that

$$\zeta_\mu = \tau_p (p/N)^2 \frac{3\pi^2 k_B T}{l^2 l_p^2}, \quad (4.3)$$

yielding (with $l^2 l_p^2 = 1.7$)

$$\zeta_\mu = \begin{cases} 17 \pm 2\tau^{-1}, & N < N_e \\ 25 \pm 2\tau^{-1}, & N > 2N_e. \end{cases} \quad (4.4)$$

Results for all our systems are presented in Table II. This is a

direct verification of the experimental finding^{3,72} and strongly supports our initial estimates of N_e . It also means that the longer chains are strongly entangled, though we are still not able to discuss the very nature of an entanglement itself. In order to be consistent, however, the lower value should coincide with the extrapolated Rouse diffusion constant

$$D_{\text{Rouse}} = \frac{kT}{N\zeta_D} \quad (4.5)$$

as found in Fig. 8. Taking the plateau value of $6ND \cong 0.4\sigma^2/\tau$ directly yields for the monomeric friction coefficient ζ_D ,

$$\zeta_D = 16 \pm 2\tau^{-1}.$$

This is not only a consistency check of the model but also means that the sample sizes considered are, in fact, large enough.

B. Long-wavelength modes: Reptation vs generalized Rouse

The relaxation of the long-wavelength modes should directly reflect the strongly decreased mobility of the long chains. This analysis also offers the opportunity to attempt to distinguish two groups of models, which have been discussed in the literature. The first is the reptation model itself which is based on the idea of relaxation in a tube. The origi-

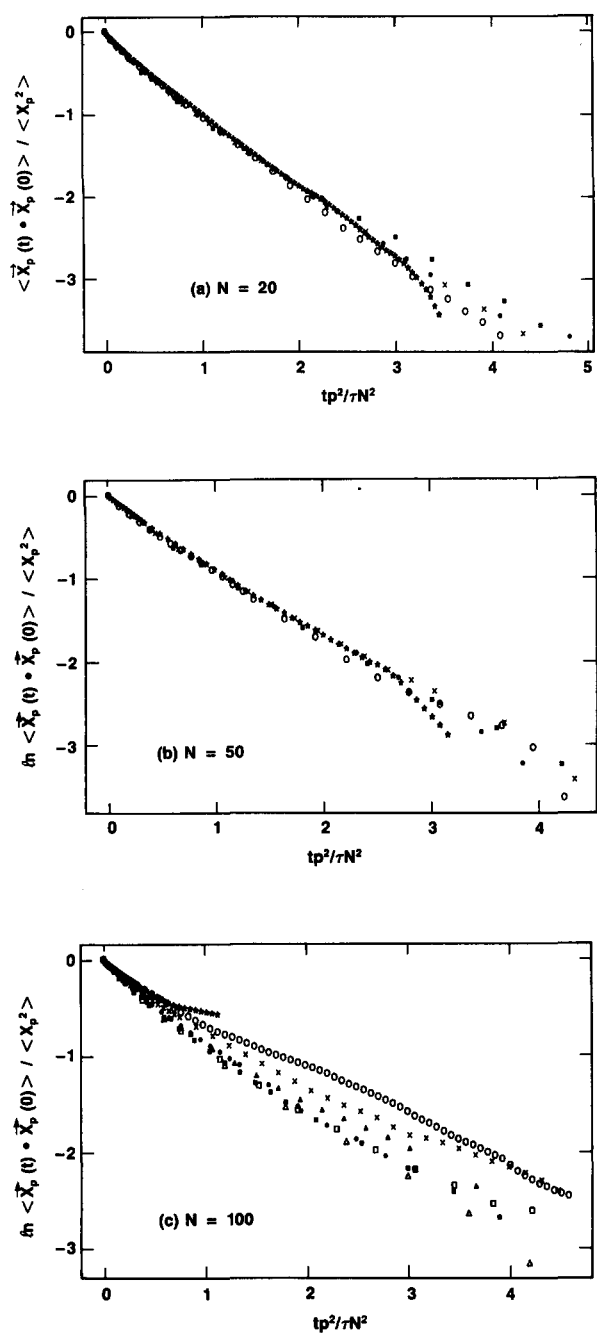


FIG. 14. Rouse plots of the mode relaxation $N/p < N_e$ for $N = 20$ (a), 50 (b), 100 (c). The symbols are the same as in Fig. 13(d).

nal relaxation time of a Rouse mode p with $N/p > N_e$ is enlarged by a factor of N/N_e , giving²

$$\tau_{p,\text{Rep}} = \frac{N \langle R^2 \rangle}{p^2} \frac{\zeta}{\pi^2 k_B T} \frac{N}{N_e} \propto N^3/p^2. \quad (4.6)$$

Hess²⁷ derived a similar expression from his microscopic model by explicitly considering the effective entanglement as a dynamic effect, which then includes constraint release/tube renewal. He finds

$$\tau_{p,\text{Hess}} = 2/3 \tau_{p,\text{Rep}} \quad (4.7)$$

after an initial fast Rouse-like decay up to the time τ_e . It is

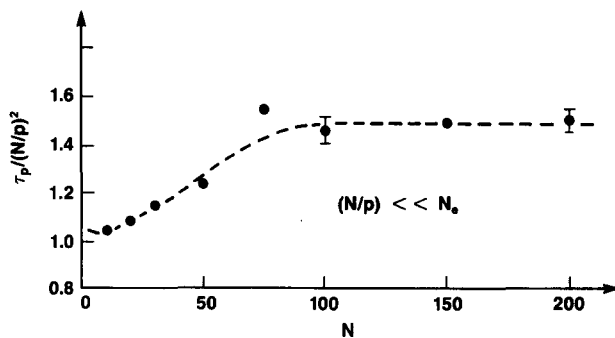


FIG. 15. Normalized decay times $\tau_p/(p/N)^2$ for $N/p < N_e$ vs N . The error bars indicate the scatter in the data from the different modes.

important to note that both models essentially describe the same physical picture. For both cases, this long-time relaxation only should occur for times larger than τ_N . For shorter times the rubber-like plateau should be observed. Ronca²⁵ employed a memory-function formalism. In the framework of Hess' self-consistent approach and the reptation model, this is a simplification containing an *ad hoc* ansatz for the time-dependent friction function. The ansatz is set to allow for a solution of the equations. Ronca's results for the time-dependent structure function (see Chap. V of Ref. 25), however, describe the motion of the chain in the frozen environment¹² rather well. There are several other approaches which can be formulated along the philosophy of Ref. 27 with the important difference that the chain-length-dependent friction coefficient becomes a static quantity.^{26,29} This also leads to a motion confined to a rather tube-like contour, depending on the time under consideration.²⁹ Contrary to this other authors claims²⁶ that this confinement only results in an overall slowing down of the motion. References 25, 26, and 28 do not give a detailed mode analysis, while Kavassalis and Noolandi²⁹ explicitly give for their generalized Rouse model (GRM)

$$\tau_{p,\text{GRM}} \propto N^3/p^4. \quad (4.8)$$

Thus an analysis of the mode relaxation should be able to exclude one of these two classes of models, though it probably cannot distinguish models within the same class.

Figure 16 shows the relaxation plots with the standard Rouse time scaling $t(p/N)^2$ for $N = 200$. One typically observes a fast initial decay followed by a significant slowing down. The curves do not exactly fall on top of one another. However, the terminal slope is the same within a factor of 1.3. Thus one has a mode-dependent crossover time to the "reptation behavior." This is in agreement with the observations that the time window to observe reptation in scattering strongly varies with p (see also Sec. V). In contrast, in Fig. 17, we plot the same data but now with a time scaling due to the generalized Rouse model as given by Eq. (4.8). Clearly, the data neither fall on one curve nor do they display the same terminal slope. For $N = 150$ and 200, in Fig. 18 the normalized relaxation times are plotted vs N . The dashed line gives the slope one would expect due to Eq. (4.8). Although the data points fluctuate, the data exclude the p^{-4} dependence of the relaxation spectra of the GRM.

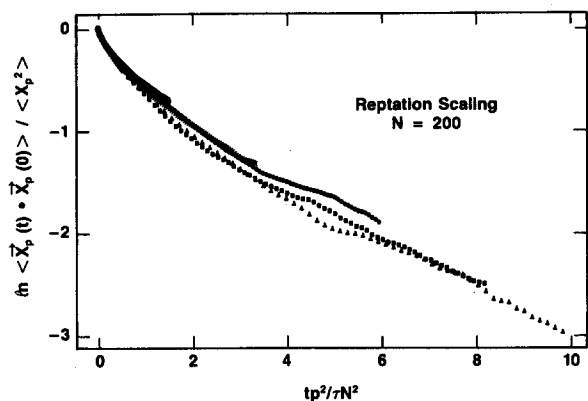


FIG. 16. Relaxation plots for $g_p(t)$ for the long-wavelength modes vs $t(p/N)^2$ (Rouse scaling) for the modes indicated for $N = 200$ ($M = 100$). The symbols are the same as in Figs. 13(d) and 17.

Are, however, the data for these chains within the crossover regime able to rule out one of the two models? In contrast to the mean-square displacement, the effect of the fast relaxing ends, as mentioned for the high p modes, only shows up in the initial drop. Thus we are correctly picking up the long-time behavior, within the time window analyzed. Nevertheless, the above time scaling of the data should for reptation only hold for $t > \tau_N$. This time is not reached by the analysis. Still the data are useful for our purpose. As seen for the single chain in a straight tube⁴² (see also the primitive chain!) the diffusional motion of the inner monomers relative to the center of mass of the chain, measured as the position along the tube, sets in at much earlier times t than τ_N . Thus, since the chain in the rigid straight tube has to show "ideal reptation," we think that the data for the relaxation of the modes rather satisfactorily follow the reptation picture. The other ansatz of the GRM uses a static p -dependent friction coefficient. For this the authors of Ref. 29 do not give an explicit crossover time for the onset of this behavior, besides $t > \tau_N$, $N/p > N_e$. Although one could argue that for the small p modes ($p = 2$) the increase in τ_p due to Eq. (4.9) might be smeared out, one at least should observe an increase in $\tau_p p^2$ for $p = 6, 5, 4$, and 3 for $N = 200$. This is not the

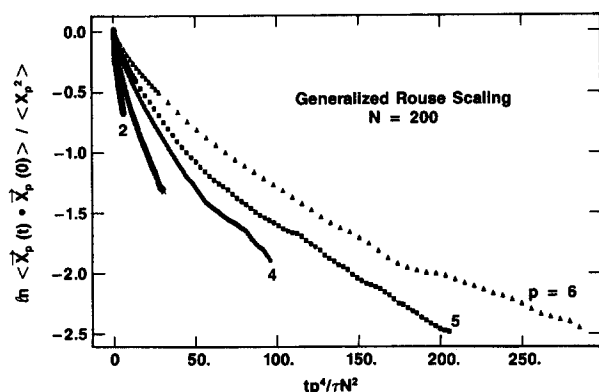


FIG. 17. Relaxation plots for $g_p(t)$ vs $t(p^4/N^2)$ (generalized Rouse model scaling). The data is the same as in Fig. 16.

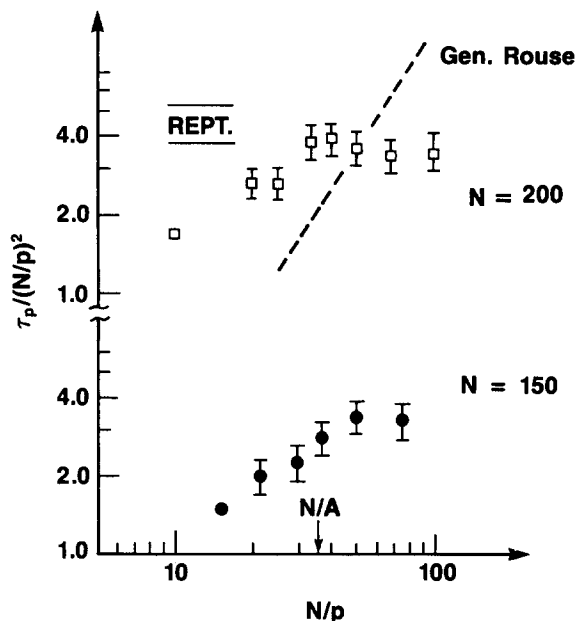


FIG. 18. Normalized relaxation times for the modes indicated for $N = 150$ and 200 ($M = 100$). The solid lines for $N = 200$ indicate the plateau for perfect reptation, while the dashed line is the expected slope for the generalized Rouse model for $N/p > N_e$.

case. Altogether we think that the data, although the chains are still in the crossover towards the highly entangled regime, strongly favor reptation-like concepts.

In the upper part of Fig. 18, the two bars give the expected value of $\tau_p(p/N)^2$ for $N = 200$ as extrapolated from the data for $N = 150$. Using Eq. (4.6), we can also directly estimate N_e from Fig. 18, giving values which are by far too large for N_e , while the crossover to the slower decay again supports our initial estimate of N_e . Similar to experiments,¹⁸ the relaxation is again too fast compared to the ideal reptation model.

Since the terminal relaxation time can only be observed by averaging over very long times, one should expect finite-size effects due to the fact that the chains are only in the crossover regime. A somewhat better situation is given for the plateau modulus G_N^0 . One can write for the time-dependent modulus

$$G_N(t) = \frac{\rho k_B T}{N} \sum_{p=1}^{\infty} \exp(-2tp^2/\tau_N), \quad (4.9)$$

where τ_N is the Rouse relaxation time. With $p^2/\tau_N = \tau_p^{-1}$, $G_N(t)$ can be estimated from the relaxation of the individual modes. The plateau modulus, following Doi and Edwards,² within the reptation theory is given by $G_N(t = \tau_e)$:

$$G_N^0 = G_N(t = \tau_e) = \frac{\rho k_B T}{N} \sum_{p=1}^{\infty} \langle \vec{X}_p(2\tau_e) \cdot \vec{X}_p(0) \rangle / \langle X_p^2 \rangle. \quad (4.10)$$

Evaluating the sum yields

$$G_N^0 = \frac{\rho k_B T}{2\sqrt{2} N} (\tau_N/\tau_e)^{1/2} = \frac{\rho k_B T}{2\sqrt{2} N_e}. \quad (4.11)$$

This result can be compared with G_N^0 calculated via Eq.

(4.9) for $t = \tau$. We get $G_N^0 = 0.0085$ ($N = 75$), 0.01 ($N = 100$), 0.014 ($N = 150$), and 0.0145 ($N = 200$). Thus for $N \geq 150$, the value of G_N^0 seems not to change very much. Analyzing $G_N(t)$ directly following Eq. (4.10), the data display a well-defined "wiggle," which increases length with chain length. However, even $N = 200$ is too short in order to use this onset of a plateau for a direct estimate of N_e . Using Eq. (4.10), we find $N_e \approx 20$. This estimate certainly is more reliable than from the long-time relaxation of the modes from a statistical viewpoint, but also from the idea that the long-chain behavior within the crossover regime for $t = 2\tau_e$ is better maintained than for much longer times. A different estimate of N_e is given by the relation for G_N^0 and the viscoelastic properties of polymeric melts. It is known that Eq. (4.10) only rigorously holds up to a prefactor of order unity. This prefactor can be estimated from viscoelastic properties. There the relaxation to the plateau modulus can be related to the tube diameter, from which one can estimate the entanglement length. Following Doi and Edwards,² for our system this would yield

$$N_e = \rho k_B T / G_N^0. \quad (4.12)$$

This equation typically is used as the definition of the entanglement molecular weight as determined from the plateau modulus. Using the data discussed above, Eq. (4.12) gives $N_e \approx 60$. This number still depends on the precise value of τ_e , taken from Fig. 9. To be on the safe side, for this estimate we chose the upper limit $\tau_e \approx 2000\tau$.

Comparing all these different estimates of N_e , the situation looks rather confusing. Clearly there is an urgent need for a clear theoretical description of what an entanglement really is. There are various criteria³⁸⁻⁴⁰ in the literature ranging from a pure packing criterium to entirely topological formulations. Kavassalis and Noolandi⁴⁰ suggest that the entanglement length only is given by packing considerations. They estimate the asymptotic N_e by calculating the average volume (blob size) which is needed to include a strand of the chain plus $\tilde{N} = 8.1$ other strands. \tilde{N} is called the coordinate number. Its average value is given by a fit to many different polymeric systems. In terms of the density ρ and l_p , their relation reads

$$N_e = [6(\tilde{N} + 1)/\pi\rho(l_p)^{3/2}(1 - N_e/N)]^2. \quad (4.13)$$

For $N \rightarrow \infty$, our estimate of $N_e = 35$ would imply $\tilde{N} \approx 4.8$, which is very small compared to other polymers investigated. Using their average value of $\tilde{N} = 8.1$ yields $N_e = 85$, which is certainly too high. However, it should be mentioned that the value of \tilde{N} varies with chemical species between 6.5 and 10.0, allowing for a large fluctuation in N_e of more than a factor of 2. There is an additional problem with Eq. (4.13). For finite N , there is a significant finite-size correction to the asymptotic value of N_e . For $N = 150$, this equation would predict that N_e is 4 times larger than for $N \rightarrow \infty$. This in turn would mean that our chains are only weakly entangled if at all. This certainly contradicts our previous results and shows the limitations of their approach. Although the chains might for a "long-time" analysis display a weaker entanglement and the analysis of the short-time-distance results might

shift us artificially towards the asymptotic limit, this seems beyond the error bars in our data.

The opposite approach is taken by Iwata and Edwards.³⁸ They tried to define the entanglements via the typical length of a chain which is needed in order to produce a knot with a strand of a different chain. They actually calculated Gaussian integrals instead of Alexander polynomials; however, that is not significant here. They found that the average strand length per winding unit is typically around 30%–40% smaller than the entanglement length determined from Eq. (4.12). This agrees almost precisely with the difference in N_e estimated from the plateau modulus via G_N^0 and from the mean-squared displacement $g_1(t)$. It might well be that looking at short times and inner monomers a remanent effect of these interwindings, which are entirely static quantities, shows up. It is certainly one of the most interesting subsequent investigations of this paper to systematically try to investigate the nature of an entanglement.

V. SCATTERING FUNCTIONS AND TUBE DIAMETER

In the preceding section, we showed that the analysis of the individual modes led to the exclusion of the generalized Rouse model. Hence in this section we will discuss the dynamic scattering function $S(q, t)$ in terms of the reptation model. This function is particularly interesting since it can be measured directly via neutron scattering and can be related to the phenomenological tube diameter d_T . The coherent scattering function for single chain is defined as

$$S(q, t) = \frac{1}{N} \sum_{ij} \langle \exp\{iq \cdot [\mathbf{r}_i(t) - \mathbf{r}_j(0)]\} \rangle, \quad (5.1)$$

and the incoherent as

$$S_{\text{inc}}(q, t) = \frac{1}{N} \sum_i \langle \exp\{iq \cdot [\mathbf{r}_i(t) - \mathbf{r}_i(0)]\} \rangle. \quad (5.2)$$

The average $\langle \dots \rangle$ indicates an average over many starting states ($t = 0$) as well as over orientations of \mathbf{q} with the same magnitude. In the present study we averaged over three orthogonal \mathbf{q} 's for each $|q|$. Note that the latter function, Eq. (5.2), is simply the Fourier transform of the single bead motion. Here the coherent $S(q, t)$ always refers to scattering from a single chain. The collective $S(q, t)$ of the overall system is not of interest here. For a discussion of correlation functions for the overall system, see Ref. 62.

Following the standard Rouse treatment of the chain relaxation of de Gennes,^{2,73} both scattering functions can be written as a function of the scaled variable $q^2(Wt)^{1/2}$. W is given by the bead friction, such that $q^2(Wt)^{1/2}$ for $t = \tau_N$ and $q \approx 2\pi/R_G$ is of order 1. Thus for chains having less than N_e monomers or small units of the longer chains as well as $q > 2\pi/d_T$, both $S(q, t)$ and $S_{\text{inc}}(q, t)$ for $k_B T q^4 (l_p)^2 t / 12\zeta \gg 1$ are given by

$$\ln S(q, t)/S(q, 0) = -q^2(Wt)^{1/2}/6, \quad (5.3a)$$

$$\ln S_{\text{inc}}(q, t) = -q^2(Wt)^{1/2}/6. \quad (5.3b)$$

The complete functional form for the Rouse model for all t is much more complicated and beyond the scope of the present investigation. The factor W can then be identified as

$$W = \frac{12k_B T}{\pi \zeta} (l_p)^2. \quad (5.4)$$

For times $t > \tau_N$ ($N < N_e$) one expects the standard diffusion behavior, namely

$$\ln S(q,t)/S(q,0) = -q^2 D t, \quad (5.5)$$

where D is the diffusion constant of the chain. In a semilogarithmic plot we expect a common curve for $S(q,t)/S(q,0)$ vs $q^2 t^{1/2}$ for $t < \tau_N$ and diffusion behavior, Eq. (5.5) for longer times. Then using the data from Fig. 15 we can explicitly compare the mode relaxation with the scattering functions. Figure 19 shows our results for $N = 75$. Here N_s is the number of scatterers per chain, positioned around the center monomer. Thus $N_s = 5$ means that only the inner five monomers had a nonzero scattering cross section. The upper panel of Fig. 19 gives $S(q,t)$ for the inner five monomers. This is essentially the incoherent scattering function since we scatter off only five monomers. The lower panel in Fig. 19 shows $S(q,t)$ for the full chain. It shows the typical Rouse relaxation. Results for different values of q scale onto a common curve up to the diffusion time. In the scaling region, the $S(q,t)$ for $N = 75$ has the form

$$\ln S(q,t)/S(q,0) = -0.33 q^2 t^{1/2}/6. \quad (5.6)$$

From Eq. (5.4), this gives a bead friction for our model of $\zeta \approx 60$, which is about a factor of 2 too large compared to that found from the diffusion and mode analysis. A similar analy-

sis for $N = 25$ gives $\zeta \approx 30$, also a factor of 2 larger than expected for short chains from our earlier analysis. Note that the ratio for the bead friction ζ between $N = 25$ and 75 is a factor of 2, similar to what we observed in Sec. IV from the mode analysis. This suggests an error in relating the prefactor relating W and ζ , Eq. (5.4) (see Sec. VI).

For $N > N_e$ and times $t > \tau_e$ the situation is much more complicated. de Gennes in his pioneering paper in 1971 (Ref. 9) discussed the coherent scattering of a reptating chain in terms of a chain in a tube of diameter d_T . The idea is simply that up to times of order τ_e one observes the standard Rouse relaxation, while for longer times, but less than τ_N the scattering function essentially sees only a smeared out chain in a tube. Thus $S(q,t)$ decays to a value which can loosely be interpreted as a Debye-Waller factor, namely

$$S(q,t)/S(q,0) = 1 - q^2 d_T^2/36, \quad \tau_e \ll t \ll \tau_d. \quad (5.7)$$

Further decay can only occur via creep out of the tube. Since the tube diameter is directly related to N_e via

$$d_T^2 = \langle R^2(N_e) \rangle, \quad (5.8)$$

we expect from Sec. III in our reduced units a tube diameter $d_T^2 \approx 60\sigma^2$. However, this plateau form for $S(q,t)/S(q,0)$ is not easy to identify. Taking the full functional form of $S(q,t)/S(q,0)$, one gets (for $t \ll \tau_d$)

$$S(q,t)/S(q,0) = 1 - q^2 d_T^2/36 + q^2 d_T^2 f[q^2 \sigma^2 (Wt)^{1/2}]/36 \quad (5.9)$$

with $f(u) = \exp(u^2/36) [1 - \text{erf}(u/6)]$, where erf is the error function. For $u \rightarrow \infty$, $f(u) \propto u^{-1}$. For later times, this changes over to

$$S(q,t)/S(q,0) \approx \left\{ 1 - \frac{q^2 d_T^2}{36} [1 - f(q^2 \sigma^2 (Wt)^{1/2})] \right\} \times \sum_{n \text{ odd}} \exp(-n^2 t/\tau_d). \quad (5.10)$$

Equation (5.10) demonstrates the difficulty in interpreting this scattering function. Kremer and Binder⁴² showed that the time, which they call the coherent time τ_{coh} , for which the plateau can be observed is strongly q dependent and varies from a minimal value

$$\tau_{\text{coh}}^{\text{min}} \propto (d_T/\sigma)^2 N \quad \text{for } q \langle R^2(N) \rangle^{1/2} \approx 1 \quad (5.11a)$$

to a maximal value for larger q

$$\tau_{\text{coh}}^{\text{max}} \propto (\sigma/d_T)^2 N^3 \quad \text{for } q d_T \approx 1. \quad (5.11b)$$

Figure 20 shows a schematic plot of $S(q,t)/S(q,0)$ for $N = 200$ for $q\sigma = 0.4$ and 0.8 using Eq. 5.10. For W we use the expression from Doi and Edwards [Eq. (5.4)] while for τ_d we take the relaxation time as expected from reptation. The bead friction is set to $\zeta = 25\tau^{-1}$ as taken from the mode analysis, Eq. (4.4). $d_T^2 = 60\sigma^2$ is taken from the mean-square displacements. From this figure it is evident that the time window to observe the plateau is rather narrow. For $q = 0.4$ no plateau at all is reached, while for $q = 0.8$ ($\approx 2\pi/d_T$) a slowing down of the decay can be seen. However, there is another complication. The above discussion only addresses ideal reptation. There are also fluctuations of

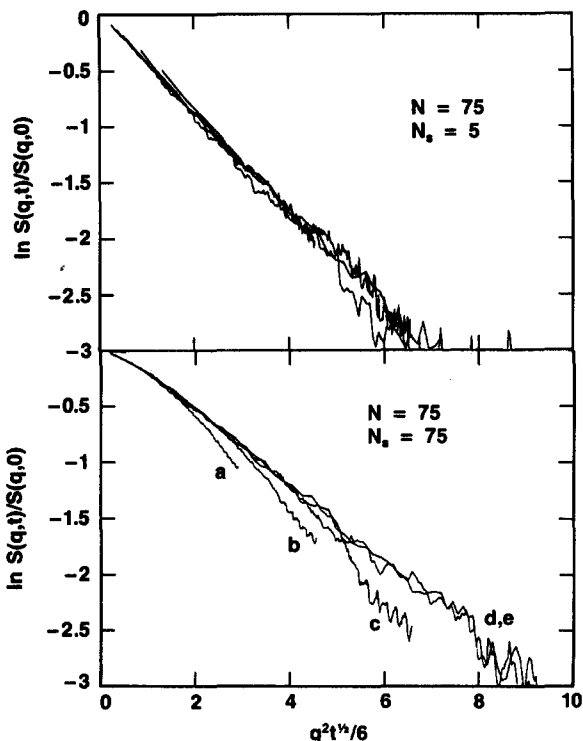


FIG. 19. Semilog plot of the coherent structure factor $S(q,t)/S(q,0)$ vs $q^2 t^{1/2}/6$ for $N = 75$ and $N_s = 75$ and 5. N_s is the number of inner monomers with a nonzero scattering cross section. The five curves correspond to different values of (a) $q\sigma = 0.4$, (b) 0.5, (c) 0.6, (d) 0.8, and (e) 1.0. The turn down at long time for curves a-c is for times beyond the Rouse regime, when the chains are simply diffusing.

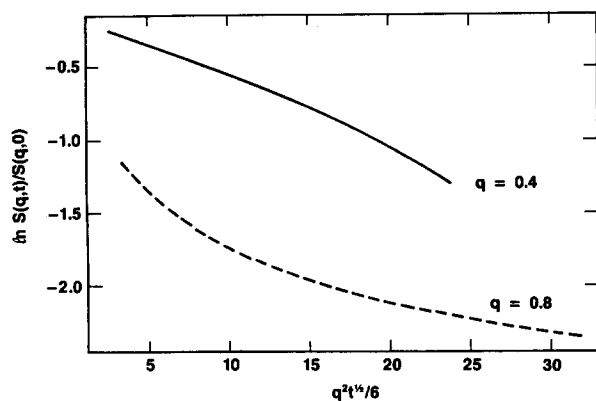


FIG. 20. Schematic plot of $S(q,t)/S(q,0)$ for $N = 200$.

the tube, they increase the “smeared out region” due to constraint release and tube leakage. This should also be taken into account. Indeed, it was already recognized for the chain moving in the frozen environment, that estimating d_T from the approximated plateau value of $S(q,t)$ gives results which are strongly q dependent.¹⁵ This was very surprising since in that case constraint release could not occur. Later analysis which compared the scattering data for the chain in the frozen environment with Ronca’s theory yielded a very reasonable estimate for d_T . Ronca²⁵ calculated $S(q,t)$ within his memory-function approach. The slowing down of the motion is governed by the memory the chain has for its previous path. Within this framework, he finds a similar plateau, however, with the form

$$S(q,t)/S(q,0) = 1 - q^4 \langle R^2(N_e) \rangle^2 / 496. \quad (5.12)$$

Figure 21 gives the results for the scattering function for $N = 150$. The upper panel shows essentially the incoherent scattering. It is important to note that the initial slope prior to where the $t^{1/4}$ regime begins is the same as for $N = 75$ (Fig. 19). The deviation from this initial decay can directly be attributed to the occurrence of the $t^{1/4}$ regime in $g_1(t)$. The characteristic time for the deviation from Rouse is typically about 30%–40% above the estimated τ_e ; however, this is difficult to determine precisely.

In order to observe the de Gennes or Ronca plateaus one has to at least have $N_s > N_e$ scatterers. The middle panel in Fig. 21 shows the result for $N_s = 35$. These data show a tendency towards a plateau, but it is rather difficult to estimate the plateau very precisely. If we assume a plateau value of roughly e^{-2} for curve c ($q\sigma = 0.6$), we find $d_T^2 = \langle R^2(N_e) \rangle \approx 86$, giving $N_e \approx 50$ using the de Gennes equation, Eq. (5.7). Within Ronca’s scheme we get $d_T^2 \approx 57$, giving $N_e \approx 34$ which agrees very well with our initial estimates of N_e from $g_1(t)$. For the other values of q , the simulations still cannot be averaged with sufficient precision far enough out in time to obtain a meaningful estimate of d_T at all. In the lower panel of Fig. 21, we give the result for scattering from the overall chain ($N_s = N$). It does not give any additional information then from the case $N_s = 35$. Considering the above discussion on $S(q,t)$ these unsatisfactory results are not surprising at all. This, however, should also be kept in mind when one interprets experimental data.

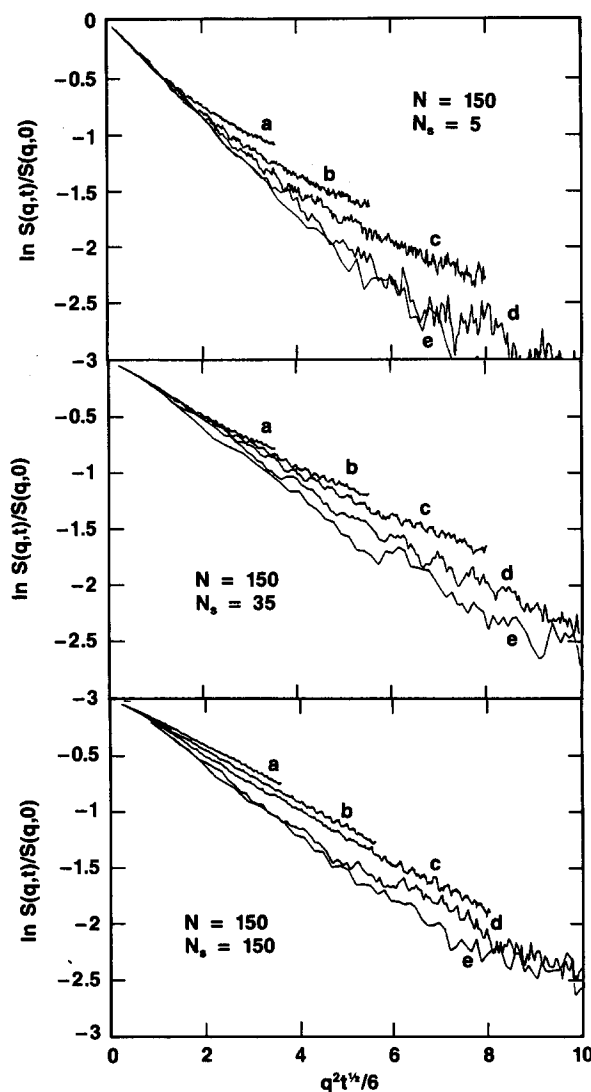


FIG. 21. Semilog plot of the coherent structure factor $S(q,t)/S(q,0)$ vs $q^2 t^{1/2}/6$ for $N = 150$ and $N_s = 150, 35,$ and 5 . In the latter two cases, only the inner N_s monomers have a nonzero scattering cross section. The five curves in each case correspond to different values of (a) $q\sigma = 0.4$, (b) 0.5 , (c) 0.6 , (d) 0.8 , and (e) 1.0 . The slowing down for long time is a clear signature of non-Rouse behavior.

VI. COMPARISON TO EXPERIMENT AND OTHER SIMULATIONS

A. Experiment

So far the discussion has been confined to a variety of physical quantities in order to provide as complete an analysis of the dynamics of entangled polymers as we could. However, one of the key problems remaining is to find a satisfactory way to determine the entanglement length N_e . In the preceding section we found that N_e determined from different measurements did not always come out the same exactly as found experimentally. Recently, it has become common practice to determine N_e experimentally by fitting data for the plateau modulus to the reptation theory (see, e.g., Refs. 3 and 5). This at least gives a consistent way to determine N_e so that different polymeric systems can readily be compared

to each other. Using our results for N_e determined in this way, together with the persistence length and the bead frictions determined earlier, we show in this section how to map our "computer" polymers onto real polymers. Doing this we cannot only compare our results to experiments but also make predictions which can be checked experimentally. One such prediction is the length scale and the time for the onset of the $t^{1/4}$ regime, which can be measured by neutron scattering.

The standard way to compare different polymeric systems with respect to their structural properties is to map the different persistence lengths. The idea is that by counting the persistence lengths provide the number of statistical segments of the chain. This should give a reasonable way to compare static properties for different polymers. Here, however, we are interested mainly in dynamic properties and it is not obvious that the mapping has to be the same. The simple mapping of the persistence length certainly gives a kind of minimal mapping, since one cannot identify units smaller than l_p with each other for polymers made up of totally different units. On the other hand, it is always possible to construct a new coarse-grained statistical segment from several persistence lengths and compare this to the persistence length of another polymer. This is simply a consequence of self-similarity of the global chain structure. If we want to include dynamic properties into our comparison, the mapping of persistence lengths is not sufficient. From the various entanglement theories for melt dynamics, it is clear that the stiffness of the chain is not the only relevant parameter in the determination of dynamical properties. Other quantities such as the microscopic bead friction are essential.

We think that there is a unique way to compare different polymeric systems including "computer" polymers. This is to map the entanglement molecular mass M_e or in our case N_e onto each other. All theories which attempt to describe the dynamics of polymer melts and especially the transition from the short-chain Rouse regime to the long-chain entangled regime introduce a new length scale into the problem, that of the entanglement length N_e . In most cases this is done without specifying what N_e physically really means. Experimentally, from linear viscoelasticity N_e is taken as a unique system specific parameter. Thus it seems natural that for different systems, N_e is the parameter which should be compared.

The most direct way to determine N_e and thus to compare our results to experiment is via the plateau moduli since data are available for many systems. Unfortunately, since our chains only contain a few N_e the analysis of G_N^0 as seen in Sec. IV does not give a very definite result for long chains. The alternative is to use the diffusion constant data. While there is not as much diffusion data available as for the plateau moduli, there are several experiments available for D of the individual chains from which N_e has been determined. In the Rouse limit, D is simply given by Eq. (4.5). The formal description of the crossover regime differ somewhat depending on the model. Nevertheless, if one knows N_e and $D(N)$ for $N < N_e$ all the curves for $D(N)/D_{\text{Rouse}}(N)$ vs N/N_e or M/M_e should fall on top of one another, if universality holds.

Before we compare our results for D to the experimental data we have to clarify one point. Experimentally, the diffusion constant D is always corrected for the N -dependent glass transition temperature T_g . This correction is especially important for systems not very far from T_g . In our case, we do not know exactly how to do this, but we think that the correction should be negligible. For a liquid of monomers interacting with a purely repulsive r^{-12} potential, Bernu *et al.*⁷⁴ estimate $k_B T_g \approx 0.4\epsilon$. The present simulations are at $k_B T = \epsilon$ and constant volume. Connecting the monomers should increase T_g . As seen from Table I, the pressure actually goes down as N is increased. This effectively produces a less dense system, partly compensating for the usual increase in T_g with increasing N . Similar in experiments, the density slightly increases with increasing chain length.⁷⁵ From numerous numerical studies of the glass transition it is clear that the fact that we can even measure the diffusion constant at all in our simulations suggests that we are *at least a factor of 2* above T_g , so that corrections to D can be neglected. In addition, as seen in Sec. IV, the variation of ζ with N is in the typical experimental range *after* the experiments have been corrected for variations in T_g . Thus we are confident that there is no correction needed.

Figure 22 shows the comparison of polystyrene (PS) of the diffusion data⁷² and polyethylene⁷⁶ (PE) compared to our model chains with $N_e = 35$ as determined from the mean-square displacement $g_1(t)$. For PS, $M_e = 18\,000$ while for PE, $M_e = 1350$ as determined from viscoelastic measurements. As the figure shows, the estimate of $N_e = 35$ gives an almost perfect match to the PE data which is determined by NMR. The PS data, obtained by forced Raleigh scattering, would suggest a somewhat larger value for N_e , about 50. However, it is not clear whether this difference is a deviation from universality in this early crossover region, which would be surprising, or whether one or both sets of data are not accurate enough. The PS data seem to show a somewhat larger scatter. Certainly our simple model is more like PE than PS. Thus for the subsequent discussion, we use $N_e = 35$, keeping in mind that PS suggests $N_e \approx 50$. Using the molecular weights of the different monomers we find

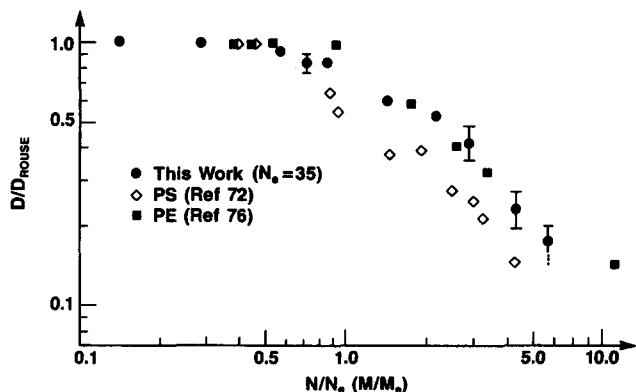


FIG. 22. Diffusion data for several polymeric liquids compared to the simulation results.

that in our model, one monomer corresponds to about 3 monomers for PE. For other polymers, the mapping is given in Table III, based on $N_e = 35$. Typically, a model monomer corresponds to several chemical beads. Polytetrahydrofuran (PTHF) (C_4H_8O)_N is an exception however. The individual bead is already a small flexible subchain with a very flexible C–O–C bond. Thus we cannot think of a bead as a rigid basic building block and we need almost two of our monomers in order to mimic one PTHF bead. In comparison to PE, this is actually not surprising.

Following this mapping procedure, we find our first important prediction. As seen from the mean-square displacements, the average distance the beads move before slowing down can be observed to be significantly smaller than the tube diameter itself, namely $3^{1/2} \approx 1.73$. This extends the range in q that one would expect to see for the slowing down by inelastic neutron scattering from $2\pi/d_T$ to $2\pi/1.73d_T$. Thus the maximal q value we would expect to see for the slowing down ranges from $2\pi/21 \text{ \AA} \approx 0.3 \text{ \AA}^{-1}$ for PTHF to only 0.056 \AA^{-1} for PS.

Nevertheless, these variations in the maximal usable q vector do not explain why some neutron spin-echo experiments seem to find a distinct slowing down of the motion in $S(q,t)$,³⁵ while others do not.¹² The reason for this can only be found in the difference in mobility of the chains for different systems. Therefore, we also need to map the time scale from our simulation onto experimental time scales so that we can then identify the crossover time τ_e at which one would expect to see slowing down and the onset of the $t^{1/4}$ regime.

For systems, where diffusion constant data are avail-

able, this mapping of the time scales is a simple exercise. Whenever the diffusion constant data are not available, we have to compare the bead friction for long chains. Since the mapping of the length scales is determined independently of the time scale, one can simply equate the Rouse diffusion constant D_{Rouse} with that determined in our MD simulation for the equivalent number of monomers. Using the length scale conversions presented in Table III, we have for PE,

$$D_{\text{Rouse}}(N=1) = D_{\text{Rouse}}(M=38.6). \quad (6.1)$$

Using Eq. (4.5) and the data from Ref. 76, this gives $\sigma^2/15\tau = 10.3 \times 10^{-5}/38.6 \text{ cm}^2/\text{s}$. Since $\sigma = 5 \text{ \AA}$ for PE, we find $\tau = 6.6 \times 10^{-11} \text{ s}$. For other systems in which D is known, the same procedure is followed. This method was used to estimate τ_e for PE and PS. For PTHF (polytetrahydrofuran) and PDMS (polydimethylsiloxane), PEP (polyethane–polypropylene), and PI (polyisoprene), the bead friction was taken from viscoelastic data for long chains^{76,77} (plateau modulus). Since the bead friction for long, entangled chains increases compared to short, nonentangled chains, we compare these data to our long-chain bead friction ($\zeta_\mu = 25\tau^{-1}$) obtained in Sec. IV. The times obtained by this mapping are presented in Table III. The typical time for the onset of the $t^{1/4}$ regime, the time where the extrapolated $t^{1/2}$ and $t^{1/4}$ regimes meet, range from $\tau_e \approx 5.5 \times 10^{-5} \text{ s}$ for PS down to $3.2 \times 10^{-9} \text{ s}$ for PTHF. Obviously, both for the simulations as well as experiments, one should not expect a sharp crossover at τ_e , rather it is meant to indicate the midrange of the crossover from the short-time Rouse regime towards the reptation regime.

TABLE III. Mapping of the bead-spring polymer model described in this paper onto experimental polymers. Assuming $N_e = 35$ and using $d_T^2 = R^2(N_e)$; the mapping procedure is described in the text. Taking $N_e = 35 \pm 5$ effects the value predicted for $g_1(\tau_e)$ and τ_e by approximately 15% and 30%, respectively. The uncertainty in the mapping for PS causes a doubling of the effective uncertainty.

| System | T | Monomer mass | M_e | Equivalent No. of beads | Equivalent mol. mass | lp | $1\sigma =$ | d_T | $[g_1(\tau_e)]^{1/2}$ | $1\tau =$ | τ_e |
|-------------------|-----------------|--------------|-------|-------------------------|----------------------|--------------------|--------------------|------------------|-----------------------|----------------------------------|--------------------------------|
| MD system | $1\epsilon/k_B$ | 1 | 35 | 1 | 1 | 1.3σ | ... | 7.7σ | 4.5σ | ... | 1800τ |
| PS ^a | 485 K | 104 | 18000 | 4.95 | 515 | 7.4 \AA | 12.6 \AA | 97 \AA | 56 \AA | $3.1 \times 10^{-8} \text{ s}$ | $5.5 \times 10^{-5} \text{ s}$ |
| PE ^b | 448 K | 14 | 1350 | 2.76 | 38.6 | 4 \AA | 5.1 \AA | 39 \AA | 23 \AA | $6.6 \times 10^{-11} \text{ s}$ | $1.2 \times 10^{-7} \text{ s}$ |
| PDMS ^c | 300 K | 74 | 9000 | 3.47 | 257 | 6.2 \AA | 8.7 \AA | 68 \AA | 39 \AA | $2.3 \times 10^{-10} \text{ s}$ | $4.1 \times 10^{-7} \text{ s}$ |
| PTHF ^d | 418 K | 72 | 1440 | 0.57 | 41 | 8 \AA | 4.6 \AA | 35 \AA | 21 \AA | $1.8 \times 10^{-12} \text{ s}$ | $3.2 \times 10^{-9} \text{ s}$ |
| PEP ^e | 500 K | 70 | 2950 | 1.20 | 84 | 7.74 \AA | 6.5 \AA | 50 \AA | 29 \AA | $0.55 \times 10^{-11} \text{ s}$ | $1.0 \times 10^{-8} \text{ s}$ |
| PI ^e | 307 K | 68 | 4100 | 1.73 | 117 | 6.6 \AA | 6.7 \AA | 51 \AA | 30 \AA | $1.0 \times 10^{-11} \text{ s}$ | $1.8 \times 10^{-7} \text{ s}$ |

^a For PS lp are taken from Ferry (Ref. 3) for PS in the \odot solvent. For the mapping the bead friction due to diffusion constant of Antonietti *et al.* (Ref. 72) was used with a consistency check with ξ_0 from viscoelasticity gave only $\sim 10\%$ deviation! Note that $N_e = 50$ would change the time mapping, giving $\tau_e \approx 2.6 \times 10^{-5} \text{ s}$.

^b Persistence length as given by Flory (Ref. 55). M_e and the diffusion constant taken from Pearson *et al.* (Ref. 75).

^c Persistence length and bead friction due to Ferry (Ref. 3). Note that the viscoelastic bead friction is obtained from entangled polymers. Thus for the Rouse diffusion equation used for comparison, we use the long-chain bead friction (Sec. IV). The data are for $T = 273 \text{ K}$. For $T = 373 \text{ K}$, τ_e changes to $1.0 \times 10^{-7} \text{ s}$, because of the strong temperature variation of the bead friction.

^d Persistence length M_e and bead friction due to Pearson (Ref. 76). Here also the long-chain bead friction has to be taken.

^e ξ , lp , and M_e from Fetters (Ref. 77). For $\xi(\text{PI})$, N_e was taken to be $2.5N_e$. $2N_e$ would reduce τ_e by about 30%.

These results shed some light on the long-standing discussion about whether neutron spin-echo scattering can be used to see the predicted plateaus in $S(q,t)$ or not. The discussion was whether the q range and time range accessible were sufficient to cover the relevant regime. The typical q range for spin echo is approximately $0.03 < q < 0.13 \text{ \AA}^{-1}$, while the longest times for which one could follow the motion was $\lesssim 10^{-8}$ s. The two most important experiments were by Richter *et al.*^{12,36} on PDMS and by Higgins and Roots³⁵ on PTHF. At 373 K, the PDMS experiments of Richter *et al.*¹² studied chains of up to $M_w = 60\,000$, which is approximately 6–7 entanglement lengths, comparable to our model chains of length $N = 200$. They scattered off the entire chain, not just the inner monomers. Therefore, it is clear from our results in Sec. III, particularly Figs. 11 and 12 and the discussion of this section, that it would be extremely difficult to observe any slowing down of the motion in those experiments at all. The ends are just too dominant for chains having N of only 6–7 N_e . Unfortunately, M_e for PDMS is only known for room temperature. Their interpretation was also questioned rather early with respect to the q range employed,⁷⁸ though we see from our results that the q range was adequate to observe deviations from Rouse, if d_T is temperature independent. More importantly, even if the chains had been longer or had they been labeled triblock chains, we estimate the crossover time $\tau_e \approx 4.1 \times 10^{-7}$ s ($T = 273$ K) and $\approx 1.0 \times 10^{-7}$ s ($T = 373$ K), respectively. Even allowing for some uncertainty in the mapping as well as in the experimental data, our results suggest that there was *no chance* to see slowing down using the older spin-echo instrument which had a limit of 10^{-8} s. Thus those early spin-echo experiments cannot be taken as evidence against reptation. We should note that more recent experiments using a newer spin-echo instrument with a maximum time limit of 4×10^{-8} s observe a deviation from Rouse towards a reduced mobility at a much higher temperature $T = 473$ K. However, these data cannot be explained by any of the current theories suggesting that there may be some problems with the T dependence of M_e for PDMS at these elevated temperatures. Additional experiments on PDMS are needed to clarify the situation. This also shows that there is a general need for an investigation of the temperature dependency of M_e . For more recent data see Note added.

For PTHF the situation is much different. Since PTHF is more flexible than PDMS, the distance scale at which the crossover to the $t^{1/4}$ regime should begin is smaller than for PDMS. This means that the available q range increases to a maximal value of approximately $2\pi/g_1(\tau_e)^{1/2} \approx 0.3 \text{ \AA}^{-1}$. The experiments³⁵ were only carried out at 0.08 – 0.13 \AA^{-1} , but should give reasonable data since they are well below this maximal q value. Unlike the PDMS samples, the PTHF samples had a much higher polydispersity. However, the chains typically contained between 20 and 40 entanglement lengths. This polydispersity certainly must have important consequences in estimating the long-time properties of the system like the terminal relaxation time, although for short-time properties around τ_e it should not play a significant role. Since the PTHF chains were significantly longer than the PDMS chains, when normalized by M_e , end effects are

not expected to be as significant. However, the crucial point is the time window. Is the motion of a single chain fast enough so that the onset of the slowing down occurs for $t < 10^{-8}$ s? Using a bead friction of 2.14×10^{-9} dynes/cm per monomer for PTHF at $T = 418$ K,⁷⁷ we find that $\tau_e \approx 3.2 \times 10^{-9}$ s, which is easily accessible by spin-echo experiments. Figure 23 is a reproduction of one of the experimental results of Higgins and Roots,³⁶ with our estimate of τ_e indicated. Here we have converted the x axis which was originally presented in amperes (since time in a spin-echo experiment is proportional to the applied Larmor precession field H) to seconds using the conversion presented in their paper. We see that our estimate of τ_e is right at the beginning of where $S(q,t)$ begins to flatten out. Thus these data clearly give direct evidence of a slowing down of the motion of the polymer chain. However, since only four very closely spaced q vectors were used and $S(q,t)/S(q,0)$ only decayed to about 0.8, the data cannot be used to distinguish which theoretical model is most applicable and to observe the expected splitting with respect to q . This also provides us with an important argument for what chain length to extrapolate the viscosity to in order to obtain ξ_μ . For PTHF Pearson⁷⁶ extrapolated $N_c = 2N_e$ in agreement to our mode analysis. There reptation and Rouse model coincide yielding a unique ξ_μ . Since ξ_μ is very sensitive to N_c , the times given for PI might be too high by about 30%–40% since there $N_c = 2.5N_e$ was taken.⁷⁷ From this we think $N_c = 2N_e$ should be the consistent choice.

The experiments on short chains of PTHF provide us with one additional important check on our simulations. Higgins and Roots⁷⁹ found that the bead friction extracted from $S(q,t)$ following the Rouse model is about twice as high as the viscoelastic data suggest. We found a similar effect in our simulations as discussed in Sec. V. This again confirms that the sample sizes and chain lengths considered in this study are sufficient.

The present mapping procedure is unique, since via the entanglement length of the various systems it is a consistent-

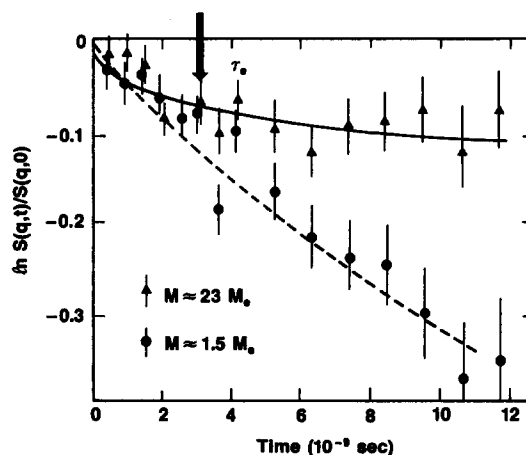


FIG. 23. Semilog plot of the coherent structure factor $S(q,t)/S(q,0)$ vs t for PTHF from Higgins and Roots (Ref. 35). For the entangled chains τ_e as found in our simulations is indicated.

ly determined quantity. Therefore, the present procedure can also be used to directly compare different experimental systems. For other simulations or the present model at different densities and/or temperatures the mapping should work equally well, considering that N_e differs for various temperatures, densities, or models.

B. Other simulations

There have been a number of other simulations which deal with the question of dynamics of polymer melts. These can essentially be subdivided into three groups. First, there are the investigations which deal with completely mobile systems in the Rouse regime.^{12–16,30} These provided a large amount of useful information for short chains with $N < N_e$. Since these studies are confined to the Rouse regime, they are not relevant here. The second group consists of a large number of studies using different approaches to test special aspects of the reptation model. These include the chain in a frozen environment,^{12,13} chain in straight tube,⁴² or a chain containing only primitive chain monomers.^{32,33,43,80} Again, since we are concerned with the validity of the reptation concept itself, this type of simulation will not be discussed here. The third group of simulations, namely those which are completely mobile and have chains long enough to reach into the entangled regime, contains up to now only three investigations. The work of Baumgärtner³¹ on Monte Carlo simulations of pearl necklace chains, the lattice Monte Carlo simulations of Skolnick, Yaris, and Kolinski,²⁶ and the present MD investigation. Baumgärtner³¹ simulated with a kink-jump algorithm a hard-sphere system at a density of $\rho = 0.7$ (bond length $l = 1$) and hard-sphere diameter $h = 0.91$. Unfortunately, only the diffusion constant and $g_1(t)$ for the inner monomers were given. Therefore, a detailed comparison of MC and MD, which would be very interesting, is not possible. However, considering Baumgärtner's data for $D(N)$, we think that there is almost a one-to-one correspondence in the number of monomers per chain in his system and ours. This is reasonable, since the hard-sphere density is only slightly lower than our density provided we measure our particle diameter as that where the interaction energy equals $k_B T$. Since his data also supports a $t^{1/4}$ power law in $g_1(t)$, we believe that the two approaches agree.

The second investigation is of a lattice polymer, which is more difficult to compare. Skolnick, Yaris, and Kolinski²⁶ simulated chains up to $N = 800$ on a simple cubic (sc) lattice at density $\rho = 0.5$. Considering the coordination number of $f = 6$ on the sc lattice, the effective density is close to that on the diamond lattice for $\rho = 0.344$ ($f = 4$) studied by one of us.¹⁵ Their chains of $N = 200$ did not show any sign of reptation. For $N = 800$, however, the authors,³⁴ when they confine themselves to the inner monomers, see an intermediate power-law regime in $g_1(t)$ of the form $t^{0.27}$. The question is how many entanglement lengths do the chains really contain. Skolnick and Kolinski argue that from the diffusion constant they get an N_e of about 110–130 using the standard equations. However, this is rather ambiguous since they do not simulate a dense melt. For their lattice density $\rho = 0.5$ on the sc lattice, they find a static screening length corresponding to a subchain of $N = 12$ monomers. So they essentially

simulate a semidilute to dense solution. Clearly the entanglement length has to be much larger than the screening length. For chains on the diamond lattice at $\rho = 0.344$ the static screening length is equal to about 15 monomers. For such a chain in a completely "frozen" environment N_e was estimated to be greater than 40. For the completely mobile system N_e of course must be much higher. In order to estimate N_e they use the diffusion constant $D(N)$. Following their publications^{16,26} one sees that DN continuously decreases starting from $N \approx 20$. As discussed above, experiments as well as the simulations of Baumgärtner and us show that DN starts to decrease around N_e . The reason their results deviate for smaller N is related to the fact that they are not at melt densities. Their chain mobility²⁶ is influenced by two effects. The first is that with increasing chain length they have a crossover from single-chain Rouse-like towards the many-chain Rouse dynamics of a dense solution. This limit is reached when the chains exceed several (5–10) screening lengths. This crossover in the present MD simulations is shifted to zero chain length. Then, with further increasing chain length, there is a second crossover from a dense solution Rouse chain to the entangled regime for the lattice polymers. Indeed a check of their diffusion data^{16,26} display a wiggle in DN vs N indicating these two effects. Thus it is impossible to estimate N_e from these data using one of the standard reptation models. However, considering this second transition region we estimate that N_e seems to be located somewhere in the range of 110–120. We think the coincidence with the previous estimates is rather accidental. This would indicate that at $\rho = 0.50$ on the sc lattice, chains of length $N = 800$ are only marginally longer, in units of N_e , than our chains of length $N = 200$. Thus it seems rather perplexing to understand why they state that their results cannot be interpreted by reptation, while our previous analysis seems to show the opposite. However, most of their conclusions are based on their attempt to see the confinement in the tube directly. Thus to check this and to show whether our chains can be seen as reptating objects or not we have to study the motion of the primitive chain, which is done in the next section.

VII. MOTION OF THE PRIMITIVE CHAIN: VISUALIZATION OF REPTATION

In the preceding section, we showed that the chain lengths considered here really do cover the crossover from pure Rouse chains for $N < N_e = 35$ to entangled chains with up to about $6N_e$ ($N = 200$). As the results show, the dynamics can reasonably well be explained by the reptation picture. The mode analysis even shows that the reptation concept seems to be more appropriate than the generalized Rouse models. Our chains also compare rather well to experimental systems. However, one intriguing question has not yet been discussed. That question is whether we can actually show the confinement on the length scale of d_T . Skolnick, Yaris, and Kolinski²⁶ claim that even for their $N = 800$ system which is roughly equivalent to our $N = 200$ chains, they could not identify any confined motion. In order to understand this, we first have to clarify under what circumstances the reptation model even predicts such a confinement. As

the test case consider the $N = 200$ system. In this case $\langle R^2 \rangle \approx 320$ giving $\langle R^2 \rangle^{1/2} \approx 18$. With $N_e = 35$ and $d_T^2 = \langle R^2(N_e) \rangle$, we get $d_T \approx 8$. Thus even for $N/N_e \approx 6$, the tube diameter is still more than about 1/3 of the total chain extension. In order to identify a motion along the contour one has to at least go to times larger than τ_e . Up to this time the monomers do not feel the constraint of the tube at all and move freely as predicted by the Rouse model up to a distance of order d_T . This means that for the direct visualization of reptation we have to disregard at least the first and last N_e monomers for each chain. Returning to our example of $N = 200$, this means that effectively only a chain of $4N_e$ is available for this analysis. If we now consider that R is only about three times larger than d_T it is obvious that chains of length $N \approx 6N_e$ cannot be used to directly visualize reptation. To do this one needs much larger chains which are beyond the present computational capabilities. Fig. 24 shows a sketch of what we have just discussed and indicates the problem for chains of order $6N_e$.

A way out of this difficulty can be found if one considers the original reptation ideas. There the motion of the primitive chain was considered and not the motion of the individual monomers. The primitive chain is a coarse-grained chain with N_e monomers per coarse-grained bead. This coarse graining was considered to be done in a way that the topological entanglements of the chain are preserved. Here we follow a slightly different approach, since the above procedure would map our $N = 200$ chain into six coarse-grained monomers. Even our longest chains of length $N = 400$ would be mapped to a system of 12 beads, hardly long enough to do any interesting analysis. Thus we construct a primitive chain (PC) in a slightly different manner by continuously coarse graining along the chain. In this procedure we subdivide the chains into $N_p = (N + 1 - N_e)/2$ subunits. The position of the new monomers is given by

$$\begin{aligned} \mathbf{R}_1 &= \frac{1}{N_e} \sum_{i=1}^{N_e} \mathbf{r}_i, \\ \mathbf{R}_2 &= \frac{1}{N_e} \sum_{i=3}^{N_e+2} \mathbf{r}_i, \dots, \\ \mathbf{R}_{N_p} &= \frac{1}{N_e} \sum_{i=N-N_e+1}^N \mathbf{r}_i. \end{aligned} \quad (7.1)$$

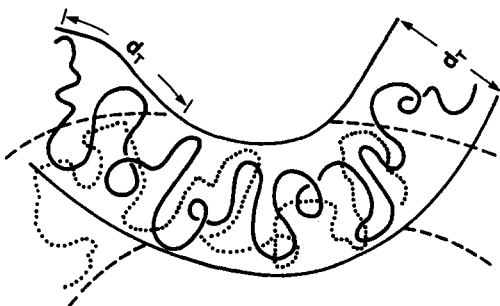


FIG. 24. Schematic sketch of the motion of a chain along its own contour. Note that the picture shows a rather stretched chain. The parameters of the sketch are set for $N = 200$, $N_e = 35$. The full and broken tubes are possible configurations about τ_e apart in time.

Note that a PC defined by Eq. (7.1) may not necessarily conserve the topology of entanglements. However, it is not clear whether the topological entanglements are relevant or what the nature of an entanglement really is. For the analysis of the motion of the PC, this does not matter since the original chain conserves entanglements. The idea now is that the PC is much more confined in its motion since it essentially has to follow the center of the tube. Thus for the inner part of the PC, we should be able to observe the reptation motion. Before we begin our analysis of the PC, we need to discuss briefly the time scales we expect to see the motion along the contour.

The reptation-like motion along the tube is supposed to take over at τ_e and to persist up to τ_d , because for $t = \tau_N$ the chain only diffused a distance of order $(N/N_e)^{1/2}$ along the tube. Thus the second $t^{1/2}$ regime should also show up in principle. However, we again run into difficulty because of our chain lengths. If Nd_T/N_e is the curvilinear length of the tube then the end-to-end distance of the PC is of order $d_T(N/N_e)^{1/2} \approx 2.4d_T$ for $N = 200$. One expects the tube to be renewed from the ends. Thus for $N = 200$, disregarding any constraint release or tube defects, after the Rouse time the tube from both ends is reduced by an amount of order $2.4d_T$ if we assume random walk statistics for the diffusional motion along the contour. Consequently, after τ_N only a small part of the tube remains even for $N = 200$, and it is therefore not possible to obtain this second regime with any reasonable accuracy. For finding the second $t^{1/2}$ regime with good accuracy N/N_e should be of the order of 100.

Before we investigate the dynamic properties of the PC, consider first its static properties. Since the PC is constructed along the chain the contour length L_p should be proportional to N_p while the contour length fluctuations should be proportional to $L_p^{1/2}$. This assumes that the PC is composed of random walk subchains. Table IV gives our results for the static properties of the PC, while in Fig. 25, we plot L_p and ΔL_p^2 vs N_p where

$$\begin{aligned} \langle L_p \rangle &= \left\langle \sum_{i=1}^{N_p-1} |\mathbf{R}_{i+1} - \mathbf{R}_i| \right\rangle \propto N_p, \\ \langle L_p^2 \rangle &= \left\langle \left(\sum_{i=1}^{N_p-1} |\mathbf{R}_{i+1} - \mathbf{R}_i| \right)^2 \right\rangle, \\ \Delta L_p^2 &= \langle L_p^2 \rangle - \langle L_p \rangle^2 \propto N_p. \end{aligned} \quad (7.2)$$

As the data in Fig. 25 show, the chains satisfy Eq. (7.2) as expected. Note that L_p has been plotted vs N_p and not N . As the table and figure indicate, the fluctuation contour

TABLE IV. Static properties of primitive chain for $N_e = 35$.

| System | N | N_p | $\langle L_p \rangle$ | $\langle L_p^2 \rangle$ |
|---------|-----|-------|-----------------------|-------------------------|
| 100/200 | 200 | 83 | 33.6 | 1152 |
| 20/200 | 200 | 83 | 32.7 | 1082 |
| 20/150 | 150 | 58 | 23.5 | 567 |
| 20/100 | 100 | 33 | 13.0 | 177 |
| 20/75 | 75 | 20 | 7.6 | 62.2 |
| 16/50 | 50 | 8 | 2.8 | 8.9 |

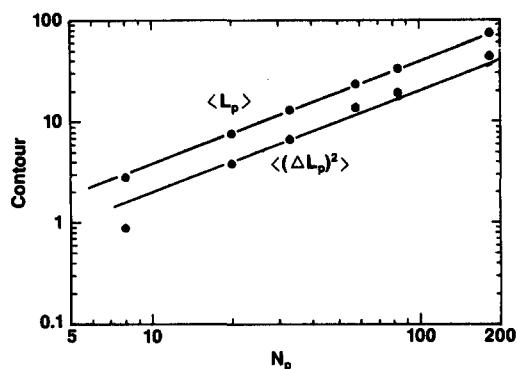


FIG. 25. (a) Mean and standard deviation of the contour length vs N_p for six chain lengths with $50 < N < 200$.

length is very small. This means that on the scale of an entanglement length the blobs containing N_e monomers repel each other rather strongly. This is important for the understanding of Rubinstein's reptation model.²¹ There in its initial form the reptons only weakly repel each other if at all. It has yet to be seen whether this interaction increases or decreases the range of the 3.4 power in the chain relaxation of this model. We, however, think that it does not destroy it, since Deutsch²⁴ found in a system where the repulsion was infinite and there was no overlap of blobs, that the 3.4 power persisted.

Now that we see that the properties of the PC length and its fluctuations follow the expected form, we can use our primitive chains for further investigations. Our aim is to find the motion along the contour, if it exists for the relatively short chains we have. To do this we first have to estimate the tube diameter d_T for the PC. Figure 26 shows $g_1(t)$ for the inner monomers for the $N = 150$ chain and for two different primitive chains constructed with $N_e = 18$ and 35. It should be clear that due to the strong mutual repulsion of the primitive path monomers the power laws for the PC are not as clear as for the full chain. The PC constructed with $N_e = 18$ is included mostly for illustration while $N_e = 35$ is the value

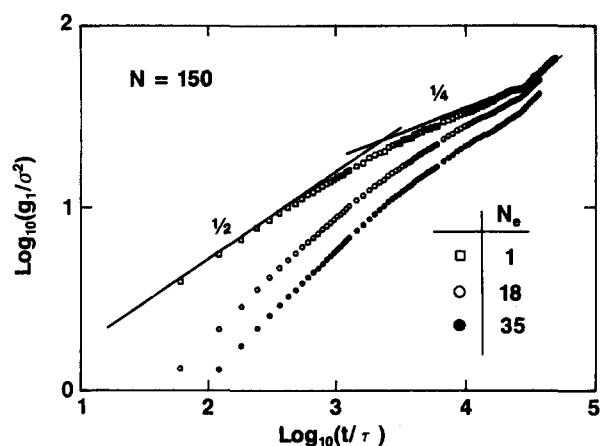


FIG. 26. Mean-square displacement $g_1(t)$ vs t/τ averaged over the inner five monomers of the primitive chain constructed with $N_e = 35$ and 18, as well as the original chain ($N_e = 1$).

expected from our previous analysis. For the original chain we know that the motion along the contour should set in at τ_e . We make the assumption that the same occurs for the PC. Again, following the reasoning described in Sec. III, $g_1(\tau_e)$ defines the tube diameter, $g_1(\tau_e) = d_T^2/3$. Using this result, we find from Fig. 26 that $g_1(\tau_e) \approx 9$ for the PC yielding $d_T \approx 5$. As expected, this value is smaller than the value obtained for the entire chain, $d_T \approx 7$. The first quantity we checked is the probability for chain elements to remain in the tube, $P_{\text{tube}}(t)$. The probability $P_{\text{tube}}(t)$ is measured as follows. Let $\mathbf{R}_i^c(t)$ be the time-averaged position of coarsened-grained monomer i at time t ,

$$\mathbf{R}_i^c(t) = \frac{\delta t}{\tau_e} \sum_{x=-\tau/2}^{\tau/2} \mathbf{R}_i(x+t), \quad (7.3)$$

where δt is the time increment of the observation or in this case the frequency at which the configurations of the entire system were written to magnetic tape for later analysis. In our case $\delta t = 60\tau$. We can then define the probability $P_{\text{tube}}(t)$ of a given monomer at time t as the probability that it is less than $d_T/2$ away from the position $\mathbf{R}_i^c(t=0)$ of the chain. Thus

$$P_{\text{tube}}(t) = P(\{\min_j |\mathbf{R}_i(t) - \mathbf{R}_j^c(t=0)| < d_T/2\}), \quad (7.4)$$

where $P(x < y)$ is the fraction of occurrences with $x < y$. This function is not unambiguous, since the correct part of the center line of the tube is not necessarily clearly defined by the averaging. The PC may also have folds in which parts of the PC are close together spatially but far apart chemically. This could lead to an incorrect estimate of $P_{\text{tube}}(t)$. To reduce this effect, we excluded all j from Eq. (7.4) which are along the contour further apart than $2g_1(t)$ of the PC. Nevertheless, $P_{\text{tube}}(t)$ only give a first impression. Figure 27 shows the result for different chain lengths and positions along the chain. Here we take $d_T = 6.25$ (only for this special quantity) in order to account for the uncertainty in definition of the middle of the tube. Figure 27(a) shows our results for the inner monomers of the PC for $N = 75$ –200. All the curves show a common decay up to a time of the order of τ_e . Then the decay for the longer chains, especially $N = 150$ and 200, becomes much slower. For $N = 150$, where we have the best statistics, the probability to stay in the original tube is about $1/2$ up to almost $3 \times 10^4 \tau$, which is nearly the Rouse time for this system ($N = 150$). From the discussion above, we would not expect this behavior to continue for much longer times. The $N = 75$ chains clearly leave the tube very rapidly. This explains why one needs at least $2N_e$ to see any effect, since for $N < 75$ the fluctuations of the ends dominate all other motion. Figure 27(b) shows in more detail what happens for chains which contain more than $2N_e$ monomers. The inner monomers are more strongly confined to the tube than the others. The outer ones try to disappear from the tube but are of course partly caught by the connectivity to the center beads. This is very similar to the results for $g_1(t)$ for various positions along the chain (Figs. 11 and 12).

A more stringent and direct test of the reptation concept is if one tries to identify the motion along the contour. Here we partially follow the analysis of Skolnick, Yaris, and Kolinski²⁶ but confine ourselves to the PC and investigate the

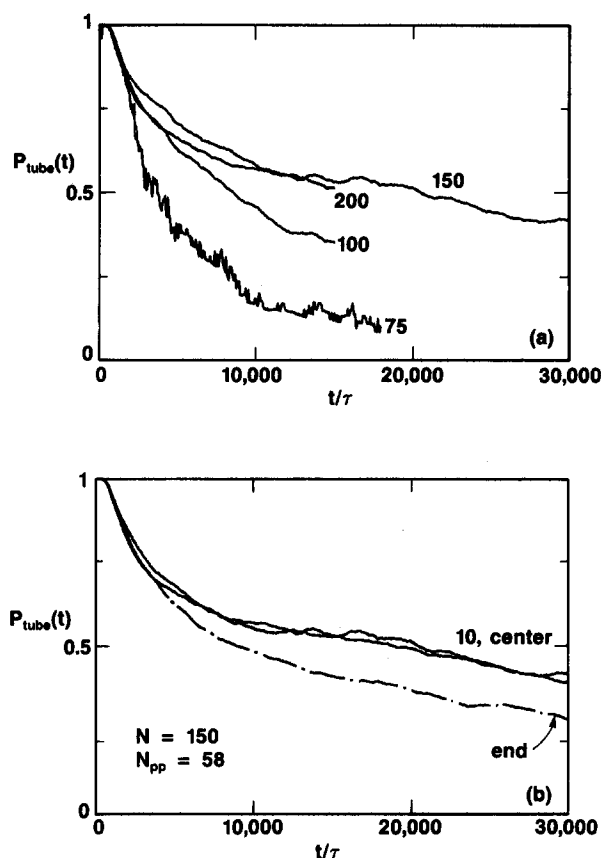


FIG. 27. Probability of staying in the tube $P_{\text{tube}}(t)$ vs t/τ for a primitive chain constructed with $N_e = 35$. The tube diameter was chosen to be $d_T = 6.25$. In (a) we show results for the middle monomer of the primitive chain for four values of N , while in (b) we present results for $N_p = 58$ ($N = 150$) for the end monomer, the 10th one from the end and center monomer.

contour motion itself. To do this one has to subdivide $g(t)$ into motion along the contour, $g_{\parallel}(t)$, and perpendicular to the contour $g_{\perp}(t)$. We can then define $g_{\parallel}(i,t)$ and $g_{\perp}(i,t)$ for each monomer i as

$$g_{\perp}(i,t) = \langle \min_h |\mathbf{R}_i(t) - \mathbf{R}_h(0)|^2 \rangle. \quad (7.5a)$$

Via $g_{\perp}(i,t)$ we identify the monomer j which minimizes $g_{\perp}(i,t)$ for a given monomer i . g_{\parallel} then is the squared contour length between monomer i and j at time $t = 0$. Disregarding contour length fluctuations, this gives

$$g_{\parallel}(i,t) = [|i-j| \langle L_p \rangle / N_p]^2, \quad (7.5b)$$

where $\langle L_p \rangle / N$ is the average bond of the PC.

For $g_{\parallel}(i,t)$ we explicitly construct the motion along the primitive path, while $g_{\perp}(i,t)$ measures the minimal distance for monomer i from anywhere along the primitive path. For the infinite reptating chain, $g_{\perp}(t)$ should be a constant while $g_{\parallel}(t)$ should follow the Rouse diffusion along the contour and thus follow a $t^{1/2}$ law up to τ_R (for the inner monomers). However, Fig. 26 shows that $g_{\perp}(t)$ for PC for $N = 150$ does not reach the $t^{1/4}$ power but only reaches an effective exponent of 0.35. Thus for $t < \tau_N$, we cannot expect a power law for $g_{\parallel}(i,t)$ with a slope lower than 0.7, if the

chains reptate. If they do not reptate, then $g_{\parallel}(i,t)$ should tend towards a constant or to the same slope as $g_{\perp}(t)$ itself. Figure 28 shows $g_{\parallel}(i,t)$ for the inner monomers of chain length $N = 50$ ($N_p = 8$) up to $N = 200$ ($N_p = 83$). For short chains ($N = 50$) the motion is isotropic almost immediately. For $N = 75$, for $t > \tau_e$ there is no sign of motion along the tube. However, for the longer chains, the situation is different. The behavior expected from reptation remains up to the longest times we can average out to, indicating a clear preference for contour motion. This picture is supported by plots of $g_{\perp}(t)/g_{\parallel}(t)$ [Fig. 29(a)] for the same inner monomers. For $N \leq 75$, $g_{\perp}(t)/g_{\parallel}(t)$ begins to increase from the earliest times shown, indicative of isotropic motion. For increasing chain length this ratio begins to decrease significantly with time. For $N = 150$, it seems to reach a very shallow minimum at about $t \approx 10^4 \tau$, while for $N = 200$ within the time we can analyze the minimal value does not appear to have been reached. Taking the value $d_T = 5\sigma$ for the tube diameter of the PC, we cannot expect much smaller values for $g_{\perp}(t)/g_{\parallel}(t)$. Figure 29(b) shows a similar analysis for different beads of the same chain. Again the end monomers need some time to feel the connectivity to a chain which moves much more slowly than the ends would like. Altogether we believe that these data nicely support the qualitative reptation picture; they do this in a way which is surprisingly clear considering the effective chain lengths we are able to study.

Finally, from the above arguments and results, it should also be possible to directly visualize the motion along the tube. To do this we simply plot projections of the configurations of a single PC onto to each other, where the configurations are 600τ apart up to a maximum of either 1.2×10^4 or $2.4 \times 10^4 \tau$. Since the tube diameter $d_T \approx 5\sigma$ for the PC constructed with $N_e = 35$, we would expect that if the chains would strictly stay in the tube, all the plotted configurations would fit into a tube of that diameter. This would then be the width of the region explored by the chains. If, however, the chains move isotropically, the width of the region covered by the configurations would be larger, given by $[3g_{\perp}(t_{\max})]^{1/2}$ for the PC. For $t_{\max} = 1.2 \times 10^4 \tau$ this gives 10. Thus there is a factor of 2 difference in the expected widths for the times

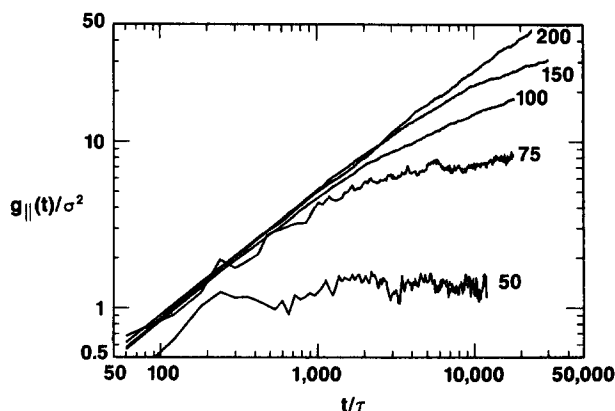


FIG. 28. Contour motion $g_{\parallel}(t)$ vs t/τ for the inner monomer of the primitive chain constructed with $N_e = 35$ for $50 \leq N \leq 200$.

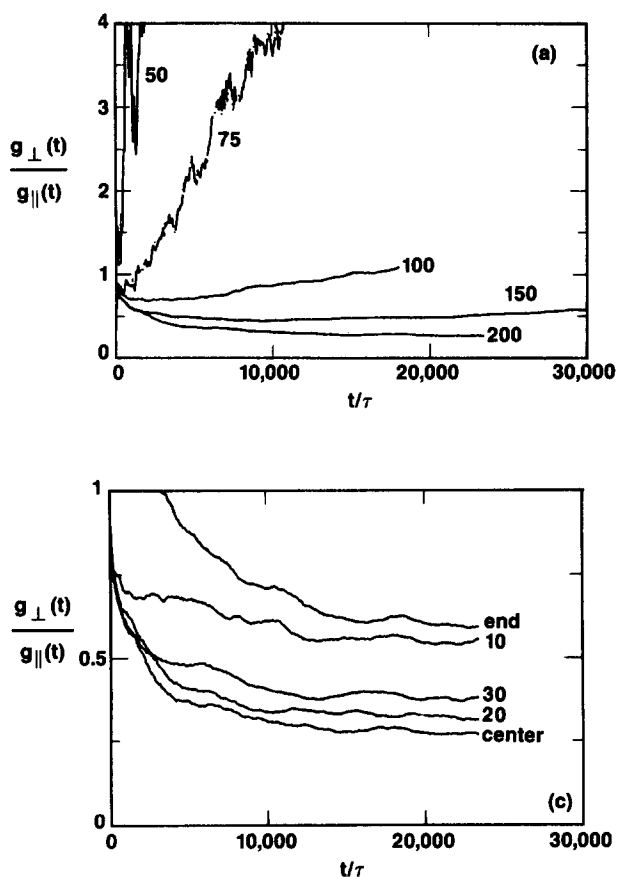


FIG. 29. $g_{\perp}(t)/g_{\parallel}(t)$ vs t/τ for the primitive chain constructed using $N_c = 35$ for (a) the inner monomer of the primitive chain for $50 < N < 200$, (b) $N_p = 83$ ($N = 200$) for the end monomer, the 10th, 20th, and 30th monomer from the end as well as the center monomer of the primitive chain. The $N = 200$ data are for the $M = 20$ sample.

considered. This should be sufficient for detecting the difference. For clarity the first 10 configurations are given as solid lines while the second 10 are dashed. Figure 30 shows the result for $N = 75$. The bars in the figure give the tube diameter (solid line) and the width of the motion for the isotropic case (dashed line). Both projections of the same chain show that there is no confinement to a tube as expected. This single sample is not sufficient to prove that the motion is isotropic but is sufficient to exclude the opposite, since the other chains show the same behavior. Figure 31 shows a similar plot for one of the $N = 200$ chains in all three projections. One clearly sees that the middle part of the chain is confined to the tube. For the entire time, both the first ten as well as the last ten configurations explore the tube but not more. One also clearly sees that the tube is slowly destroyed and/or renewed by the motion of the chain ends. This can be seen as the classical tube renewal process.² For the time covered here the tube length remaining is reduced by a factor of $2-3d_T$ in agreement with our previous discussion. While Fig. 31(a) gave the three projections of the same chain, Fig. 31(b) shows examples for three different chains. Again, we find the expected behavior for two of the chains. However, we also see that one chain certainly deviates from reptation.

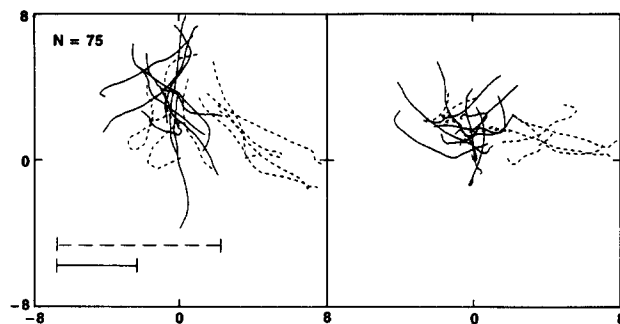


FIG. 30. Two projections of the configuration of one of the primitive chains for $N = 75$. The projections were plotted every 600τ . The first ten were plotted as solid lines and the second ten as dashed lines. The center of mass of the first configuration was placed at the center of the box. The horizontal dashed bar is the amount the chain moves during the elapsed time of $12\,000\tau$ as determined by $g_{\perp}(t)$ assuming isotropic motion, while the solid line is the tube diameter determined from the onset of the $t^{1/4}$ regime in $g_{\perp}(t)$ (Fig. 9) for large N .

In that case, there is obviously some tube leakage or constraint release. Since we only found one such chain it is impossible to estimate the statistical significance of this in more detail.

In order to be able to prove that these effects are real and independent of chain length, we also simulated a system of $N = 400$. Figure 32 shows three projections for the same chain. The result is as expected. Again the middle part of the chain is strictly confined to the region of the proposed tube diameter. The size of the region of enhanced mobility is constrained to the same amount of outer beads as for $N = 200$. A very interesting aspect is given by the middle example in Fig. 31(a). There either the tube had in the beginning some leakage or a constraint changed during the course of the run. It looks as though part of the chain was pulled (back) into the tube by the rest of the chain. For illustration, Fig. 33 shows a three-dimensional plot for two $N = 400$ chains for $24\,000\tau$.

Although the original chains are too short to be used to visualize the tube directly, we can do this by examining the PC. Besides an occasional observation of tube leakage and/or constraint release, which is included in more recent modifications of the reptation theory, the motion of the PC is very much like what one expects from the original reptation picture. It is clear that the analysis of this section cannot be taken as evidence for or against any specific model; for this we have to return to the discussion in Sec. III. However, what the analysis in this section shows is that the original reptation idea of the motion on a coarsened-grained scale is clearly evident for the present chain lengths and that they give a very good qualitative impression of the motion of the chain.

VIII. SUMMARY AND CONCLUSIONS

In the present paper, we have presented a rather extensive study of the dynamics of a polymeric liquid far above the glass transition temperature. The paper contains three main results:

(i) At the level of a single chain, reptation provides a very good description of the dynamics of long, entangled

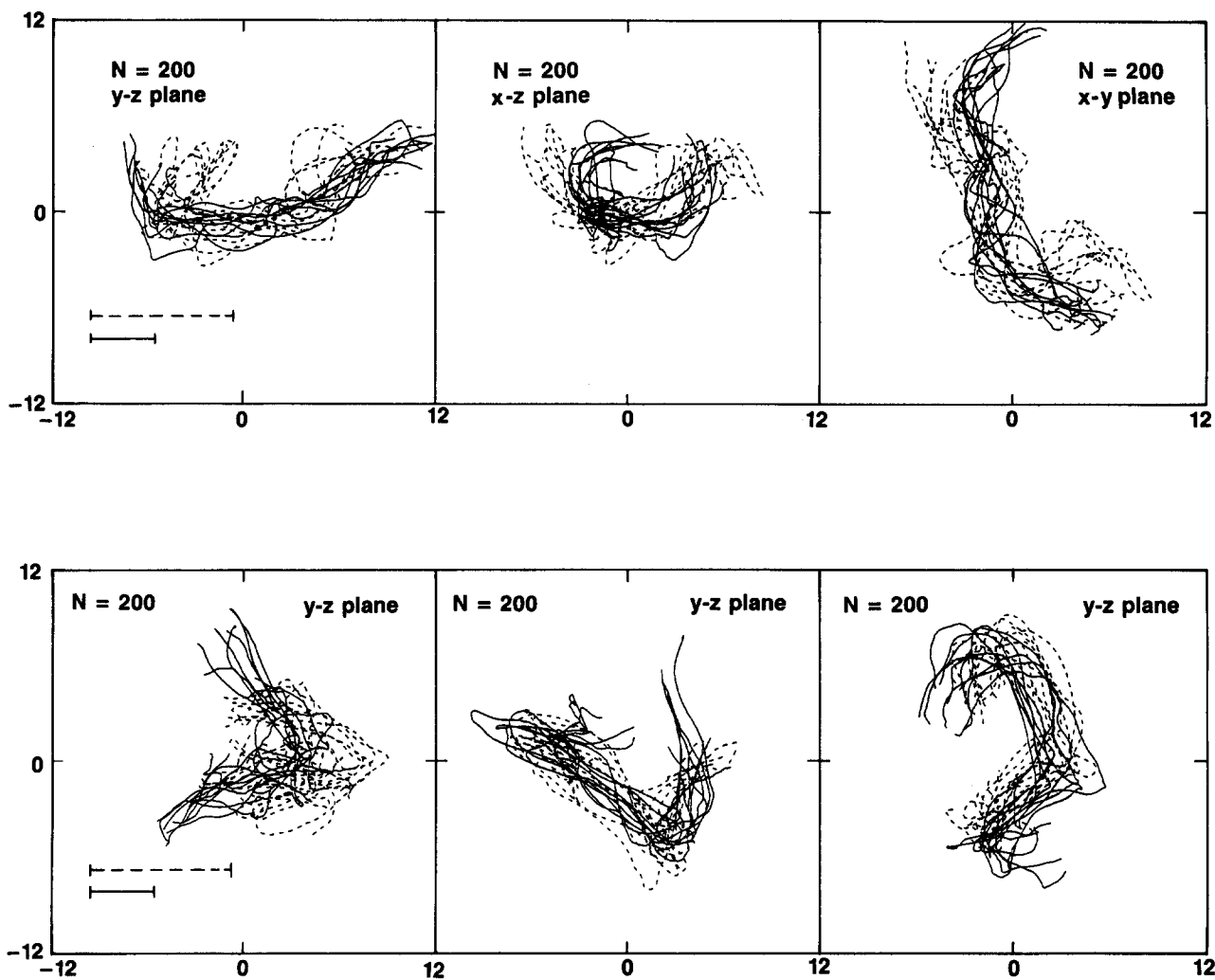


FIG. 31. Same as Fig. 30 for $N = 200$. (a) Three projections of the same primitive chain and (b) the projection onto the y - z plane for three other chains. In all cases the center of mass of the first projection was shifted so that it was at the center of the box. Note the development of a well-defined tube in comparison to Fig. 31. Total elapsed time is $12\,000\tau$, which is still in the $t^{1/4}$ regime for $N = 200$.

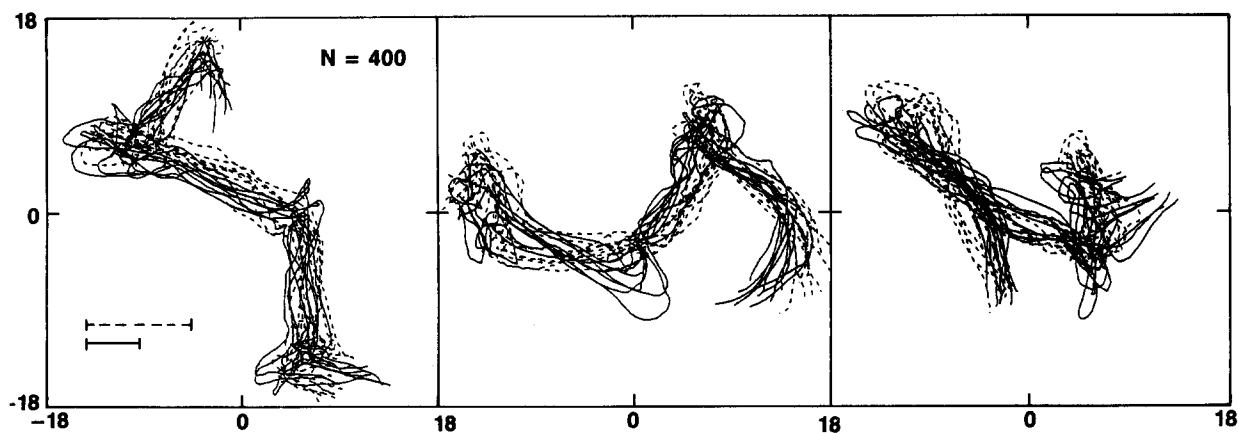


FIG. 32. Same as Fig. 30 for $N = 400$. Here we show three projections of the same primitive chain. As in Fig. 30, the first 10 projections are plotted as solid lines, while the second 10 are dashed. Total elapsed time $12\,000\tau$.

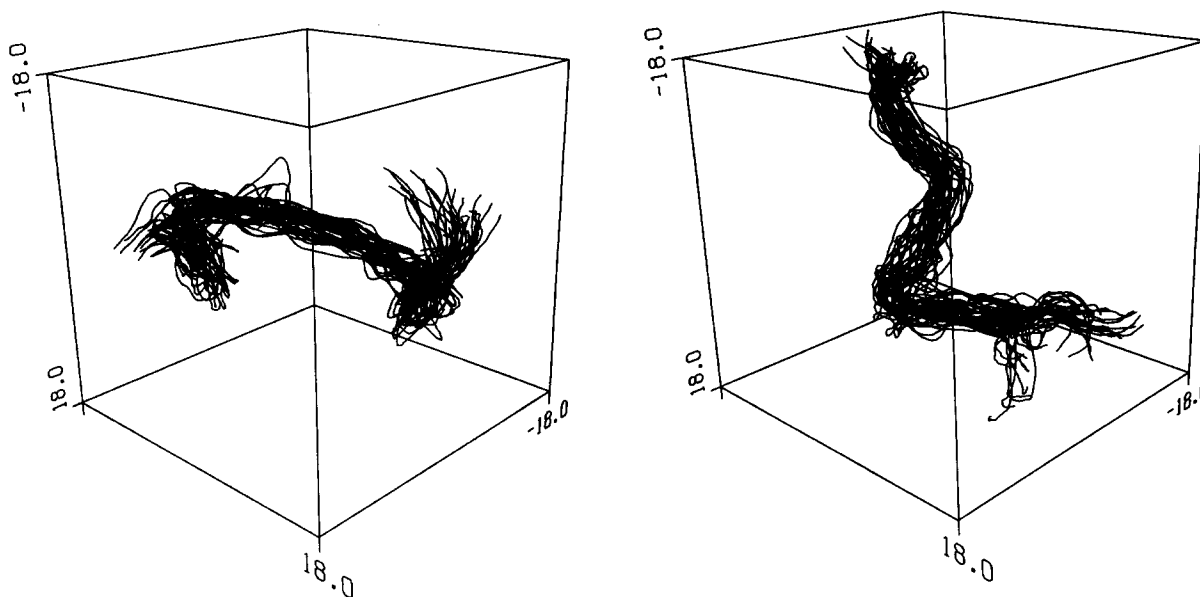


FIG. 33. Configurations of the primitive path of two different chains for $N = 400$. The contours are plotted every 600τ and the total elapsed time is $24\,000\tau$. As in the previous plots the center of mass of the first configuration for each chain is shifted to the center of the box for purposes of illustration.

chains, while the Rouse model provides an excellent description for short chains.

(ii) By mapping our polymers to experimental polymeric liquids, we find that N_e can be estimated uniquely, and we are able to resolve a long-standing controversy regarding the interpretation of neutron spin-echo experiments.

(iii) By analyzing the motion of the primitive chain, we have shown that it is possible to directly visualize the confinement of the motion of a chain within a tube even for the chain lengths considered here.

By using a very simple model system, we have been able to study chain lengths which cover the crossover from Rouse behavior into the reptation regime. This is the first extensive study of this kind using molecular-dynamics methods. The first main result of this work is that as long as we consider the motion of a single chain, the data agree very well with the reptation model. This is surprising since we mainly cover the crossover regime where the chains contain only a few N_e . The mean-square displacement $g_1(t)$ clearly exhibits a slowing down of the motion, which can be taken as a $t^{1/4}$ power law. Here it is important to consider the different mobilities of the monomers, depending on where they are situated along the chain. This explains why other investigations did not observe the $t^{1/4}$ regime.²⁶ Since there are several models in the literature which suggest a slowing down in the motion of a monomers, we performed a detailed analysis of the Rouse modes in order to aid in clarifying which works best. The reptation^{8-10,17} model and the more microscopic approach of Hess²⁷ propose a mode spectrum which agrees with our results, while the generalized Rouse models,²⁹ which introduce a chain-length-dependent increased static friction, yield a different spectrum. From this analysis, we have to conclude that the reptation model and reptation-like models provide a better description of the motion. The interpretation of the scattering function $S(q,t)$ is more difficult.

Again, one faces problems related to the mobility of the chain ends. Also the onset of the creep term, which is strongly q dependent, causes problems. Thus here we were mainly confined to the incoherent scattering, which again showed clear evidence for slowing down of the motion.

The second important aspect of this work is concerned with comparison of the simulation results to experiment. We showed, by mapping the entanglement length N_e to the entanglement mass M_e , that the results of such a conceptually simple model can be used to make definite predictions for many different chemical species. We showed that while the time scales for the slowing down of the motion to set in were out of the range for the neutron spin-echo spectrometer available a few years ago (by a factor of 10) for PDMS, the crossover time was within the range for PTHF. The actual value of τ_e for PTHF agrees very well with the measurements by Higgins and Roots.³⁵ It is impossible to perform simulations for the time and distance scales considered here for models containing all or many chemical details. It also will not be possible for a few generations of future computers. For this reason, simulations of coarse-grained models such as the one considered here and a mapping to experimental parameters is very important. One may even argue, based on the success of the present model, how useful a simulation on a detailed model would be for the problems under investigation here. We believe that a more useful strategy would be to obtain precise experimental and theoretical results for short chains, and then extrapolate to longer chains using the results of a simulation for a very simplified model like the one considered here. The present work is only the first step in this direction, but we think a rather promising one.

The third main result of the present paper is the analysis of the motion of the primitive chain. We showed that for chains which are several times longer than N_e , the probabili-

ty of staying in the tube decays very slowly for the inner monomers and the motion along the contour becomes significant. However, the most direct check of this behavior is given by the direct visualization of the reptation motion. By simply plotting several configurations of a chain at a fixed time interval, it is possible to directly verify that the chains move in a tube. From this aspect of our work we also concluded that the original reptation concept works very well.

Obviously there still remain many open questions which need to be addressed in future research. One of most importance is the origin of the $N^{3.4}$ power law for the viscosity. There have been a number of explanations which are based on a many-chain picture as well as some which remain within the classical reptation framework. Rubinstein, e.g., discusses the motion of subunits of N_e monomers, called reptons.²¹ In his approach reptons can easily sit on top of one another. However, this does not agree very well with our results for the mean-square displacements of the primitive chain, which we discussed in Sec. VII. There it appeared that the "reptons" strongly repel each other, more in agreement with Deutsch's earlier reptation simulation algorithm.²⁴ However, this model had the unphysical aspect that a subunit of N_e monomers occupied the space $\langle R^2(N_e) \rangle^{d/2}$ exclusively. Thus more work is needed to clarify this point, though it probably cannot be done using an approach at the microscopic level of the present simulation. In a similar manner, the present approach cannot yield statistically significant information on tube leakage-constraint release, at least on the computers presently available. Here we can only say that such events can be observed as we did by directly looking at the motion of the primitive chains.

One additional aspect which deserves closer attention is the very nature of the entanglement lengths. There are many concepts, ranging from purely topological arguments to purely packing ideas, which need further testing.³⁷⁻⁴⁰ Also, the PDMS experiments indicate a strong temperature dependency of M_e . This is not included in any of the current theories. This problem is one which can be solved with the help of the present simulation techniques and we plan to do more on this problem in the future.

Besides the direct extensions of the present work to systems of longer chains or systems with polymers of more than one chain length, the methods developed here and the reference systems investigated open the way to studying much more complex structures, such as networks and rubbers. Such investigations are currently under way and we will report the results in future publications.⁶⁵

Note added

After completing this work we received two preprints by Schweizer on a mode-coupling theory of polymeric liquids.⁸⁵ His approach yields partially results, which are similar to reptation. Instead of a $t^{1/4}$ regime he finds $t^{9/32}$. This certainly fits our data as well. The crucial test of the theory lies in the mode relaxation τ_p . There Schweizer's results differ significantly from reptation yielding effectively p -independent relaxation times for large N . However, since this form of the equation is only applicable for $t \gg \tau_N$, $N \gg N_e$ the simulations by now cannot cover this regime. Our analysis in Sec. IV,

however, indicates good agreement with reptation theory.

Very recently, experiments on PEP (Ref. 86) extended the early results significantly on PTHF (Ref. 35) and PDMS (Ref. 36) to the limit that a separation of plateau values for different q could be observed. This is the first microscopic experiment, which can be used to identify a tube diameter d_T . Richter *et al.*⁸⁶ found a crossover to a plateau value in $S(q,t)$ for various q vectors. Their data are not capable of distinguishing Ronca's asymptotic scattering function from the one of de Gennes's (see Sec. V). We included PEP in Table III, showing that for the new spin-echo instrument (resolution $\sim 4 \times 10^{-8}$ s) a well-defined slowing down of the motion had to be expected to be seen. Note that the old experiments, used for PTHF (Ref. 35) and PDMS (Ref. 12) had a resolution of only up to 1.2×10^{-8} s.

ACKNOWLEDGMENTS

During the course of this work, we had valuable discussions and obtained important insight from many colleagues, especially K. Binder, I. Carmesin, B. Dünweg, L. J. Fetters, W. W. Graessley, D. S. Pearson, P. A. Pincus, N. Pistor, D. Richter, H. Sillescu, and T. A. Witten. We acknowledge the support of a NATO travel grant No. 86/680. K.K. acknowledges the hospitality of Exxon Research, and G.S.G. that of Universität Mainz and Forschungszentrum Jülich. These calculations were made possible by a generous grant of CPU time from the German Supercomputer Center HLRZ, Jülich.

APPENDIX

We simulated our systems at constant density in a cubic cell with periodic boundary conditions. Each chain consisted of N monomers connected by an anharmonic spring.^{4,14,52} All the monomers interacted with a repulsive Lennard-Jones potential,

$$U_{ij}^{LJ} = \begin{cases} 4\epsilon [(\sigma/r_{ij})^{12} - (\sigma/r_{ij})^6 + \frac{1}{4}], & r_{ij} \leq 2^{1/6}\sigma \\ 0, & r_{ij} \geq 2^{1/6}\sigma, \end{cases} \quad (A1)$$

where r_{ij} is the distance between monomer i and j . For monomers which are neighbors along the sequence of the chain, we added an attractive potential (FENE potential⁴)

$$U_{ij}^{ch} = \begin{cases} -0.5kR_0^2 \ln [1 - (r_{ij}/R_0)^2], & r_{ij} \leq R_0 \\ \infty, & r_{ij} \geq R_0 \end{cases} \quad (A2)$$

This general form for the potential between connected monomers has been used previously.^{4,14} However, for our purposes we had to use different parameters for k and R_0 in order to avoid any bond crossing. For the present simulation, as in our previous simulations using this model,⁵²⁻⁵⁴ we used $R_0 = 1.5\sigma$ and $k = 30 \epsilon/\sigma^2$. This spring constant was strong enough so that the maximum extension of the bond was always less than 1.2σ for $k_B T = 1.0\epsilon$, which made bond crossing energetically infeasible. (The maximum extension of the bonds was monitored during the course of the simulation in order to be assured that no crossings occurred.) However, k was also small enough so that we could use an integration time step Δt , which is comparable to what one would use for a fluid of Lennard-Jones particles. Increasing k

would reduce the maximum extension further but would require a reduction in Δt . We explored a number of values for k and R_0 and found this set to be a convenient compromise, not so stiff that we had to use too small a time step, yet not so soft that bond cutting was possible. Most of our simulations the equations of motion were integrated using a fifth-order predictor-corrector algorithm due to Gear,⁸¹ though we also made some runs using the third-order predictor-corrector. Both orders gave the same results, though the third order was approximately 10% faster.

As mentioned in Sec. II, we coupled the monomers weakly to a heat bath both to keep T near its preset value but also to keep the temperature from drifting upward due to numerical roundoff errors which always begin to accumulate whenever one makes runs longer than a few million time steps. We solved numerically the equation of motion, given by Eq. (2.1). The white-noise source and the bead friction Γ are related by

$$\langle \mathbf{W}_i(t) \cdot \mathbf{W}_j(t') \rangle = \delta_{ij} \delta(t - t') 6k_B T \Gamma. \quad (\text{A3})$$

The temperature T can then be set, and during the course of the run will fluctuate around the preset value. We are thus essentially simulating a canonical ensemble. The value of Γ we used was $0.5\tau^{-1}$, where $\tau = \sigma(m/\epsilon)^{1/2}$. This value was convenient since it had to be small enough not to produce Rouse-like behavior on length and time scales of the order of a bond length, but large enough to stabilize the system at long time scales. We estimate that values in the range $0.1 < \Gamma < 1.0$ would work equally well.^{52,53} If Γ is too large any numerical algorithm for integrating second-order differential equations will break down since the random noise and viscous damping terms in Eq. (2.1) would then dominate over the inertia term. For very short times (a few Δt), an MD simulation has the advantage that monomers move cooperatively and ballistically, which is more effective than in a MC simulation. However, because our system is dense, the long-time diffusion is dependent only on the interactions between monomers and does not arise from the Langevin terms in the equation of motion. That is, the observed monomeric friction coefficient $\xi \gg \Gamma$ (see Sec. III). The Langevin terms in the equation of motion do, however, give rise to an overall diffusion of the center of mass of the entire system. Using the Einstein relation, one expects that the diffusion constant of the entire system D_{tot} will have the form

$$D_{\text{tot}} = k_B T / \Gamma MN, \quad (\text{A4})$$

where MN is the total number of monomers in the system. This gives $D_{\text{tot}} = 2/MN$ in our case. Thus in order to find the individual chain diffusion we removed this diffusion from all quantities, like $g_i(t)$, $S(q,t)$, etc. For each system we also measured D_{tot} directly and found that it agreed with Eq. (A4) to better than $\pm 5\%$. In all cases the fluctuations of the measured diffusion constants for the total system was at least an order of magnitude smaller than the diffusion constants of the individual chains. For $N = 100$ and 150 , where the errors in D are larger than for smaller N , the relatively large uncertainty in D for the individual chains comes from the scatter in the data for the individual chains themselves and not from the effect of the overall diffusion of the whole

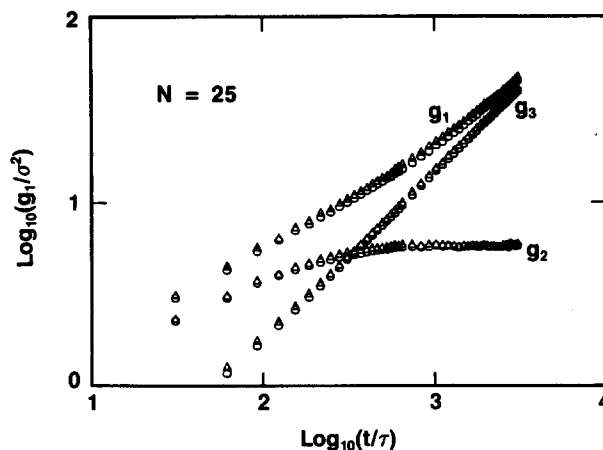


FIG. 34. Comparison of the mean-squared displacements $g_1(t)$, $g_2(t)$, and $g_3(t)$ for $N = 25$ for two simulation techniques. Results for $g_1(t)$ and $g_2(t)$ are averaged over the inner five monomers. The open triangles are for the molecular-dynamics simulation in which the monomers are coupled weakly to a heat bath, with $\Gamma = 0.5\tau^{-1}$, while the open circles are for the case in which the temperature is scaled every 100 steps such as to keep the energy constant. Both simulations were run to $12\,000\tau$ with $\Delta t = 0.006\tau$. Clearly both methods for stabilizing the system for long times give the same result.

system. For $N = 200$ we use the large 100/200 system to estimate D .

As an additional check we compared the results of a simulation of $M = 32$, $N = 25$ using the method described above with the results of a simulation with $\Gamma = 0$, but in which the velocity was rescaled every $100\Delta t$ in order to keep the total energy of the system constant. The total run for each case was $12\,000\tau$ and Fig. 34 shows the results for $g_i(t)$ ($i = 1, 2$) averaged over the inner 5 monomers and for $g_3(t)$ for the two methods. As can be seen, there is no significant difference within the statistical scatter in the data. Similar results were found using different methods in the course of our work on simulating colloidal particles.⁸²

We also made a run of 1200τ in which the velocity was rescaled each time step so that $\langle v^2 \rangle = 2k_B T/3$.⁸³ After about $10^6 \Delta t$, the internal temperature of the system began to cool down. Because this form of temperature control does not keep the total momentum of the system zero, eventually for very long runs the random fluctuations lead to an ever increasing total momentum for the entire system. This has not to our knowledge been observed in previous simulations since the runs were typically much shorter. Had we rescaled the velocities in such a way that the total momentum of the system remained zero, we expect we would have obtained results in agreement with those presented here.

The programs were optimized to run very effectively on the Cray XMP. A general description of such a program is given in Ref. 84. Besides what is mentioned there, the calculation of forces along the sequence of the chain was taken into a separate loop which vectorized trivially.

¹P. G. de Gennes, *Scaling Concepts in Polymer Physics* (Cornell Univ. Press, Ithaca, NY, 1979).

²M. Doi and S. F. Edwards, *The Theory of Polymer Dynamic* (Clarendon, Oxford, 1986).

- ³J. D. Ferry, *Viscoelastic Properties of Polymers* (Wiley, New York, 1980).
- ⁴R. B. Bird et al., *Dynamics of Polymeric Liquids* (Wiley, New York, 1977), Vols. 1 and 2.
- ⁵D. S. Pearson, *Rubber Chem. Technol.* **60**, 439 (1987).
- ⁶W. W. Graessley, *Stud. Polym. Sci.* **2**, 163 (1987); *Adv. Polym. Sci.* **47**, 67 (1982).
- ⁷P. E. Rouse, *J. Chem. Phys.* **21**, 1273 (1953).
- ⁸S. F. Edwards, *Proc. Phys. Soc.* **92**, 9 (1967).
- ⁹P. G. de Gennes, *J. Chem. Phys.* **55**, 572 (1971).
- ¹⁰P. G. de Gennes, *J. Chem. Phys.* **72**, 4756 (1980).
- ¹¹K. Kremer, G. S. Grest, and I. Carmesin, *Phys. Rev. Lett.* **61**, 566 (1988).
- ¹²D. Richter, A. Baumgärtner, K. Binder, B. Ewen, and J. B. Hayter, *Phys. Rev. Lett.* **47**, 109 (1981); **48**, 1695 (1982).
- ¹³A. Baumgärtner and K. Binder, *J. Chem. Phys.* **75**, 2994 (1981).
- ¹⁴D. Ceperly, M. H. Kalos, and J. L. Lebowitz, *Phys. Rev. Lett.* **41**, 313 (1978); M. Bishop, D. Ceperly, H. L. Frisch, and M. H. Kalos, *J. Chem. Phys.* **76**, 1557 (1982).
- ¹⁵K. Kremer, *Macromolecules* **16**, 1632 (1982).
- ¹⁶A. Kolinski, J. Skolnik, and R. Yaris, *J. Chem. Phys.* **84**, 1992 (1987); **86**, 1567 (1986); **86**, 7164 (1987), and references therein.
- ¹⁷M. Doi and S. F. Edwards, *J. Chem. Soc. Faraday Trans. 2* **74**, 1789 (1978); **74**, 1802 (1978); **74**, 1818 (1978); **75**, 38 (1978).
- ¹⁸R. H. Colby, L. J. Fetters, and W. W. Graessley, *Macromolecules* **20**, 2226 (1987).
- ¹⁹M. Doi, *J. Polym. Sci., Polym. Lett.* **19**, 265 (1981); *J. Polym. Sci., Polym. Phys. Ed.* **21**, 667 (1983).
- ²⁰J. des Cloizeaux, *J. Phys. (Paris) Lett.* **45**, L17 (1984); R. J. Needs, *Macromolecules* **17**, 437 (1984).
- ²¹M. Rubinstein, *Phys. Rev. Lett.* **59**, 1946 (1987).
- ²²H. Scher and M. F. Schesinger, *J. Chem. Phys.* **84**, 5922 (1986).
- ²³H. Wendel and J. Noolandi, *Macromolecules* **15**, 1313 (1982).
- ²⁴J. M. Deutsch, *Phys. Rev. Lett.* **54**, 56 (1985).
- ²⁵G. Ronca, *J. Chem. Phys.* **79**, 1031 (1983).
- ²⁶J. Skolnick, R. Yaris, and A. Kolinski, *J. Chem. Phys.* **88**, 1407 (1988); J. Skolnick and R. Yaris, *ibid.* **88**, 1418 (1988).
- ²⁷W. Hess, *Macromolecules* **19**, 1395 (1986); **20**, 2589 (1987); **21**, 2620 (1988).
- ²⁸M. Fixman, *J. Chem. Phys.* **89**, 3892 (1988); **89**, 3912 (1988).
- ²⁹T. A. Kavassalis and J. Noolandi, *Macromolecules* **21**, 2869 (1988).
- ³⁰C. C. Crabb and J. Kovac, *Macromolecules* **18**, 1430 (1985); and more recently, C. C. Crabb, D. F. Hoffmann, M. Dial, and J. Kovac, *Macromolecules* **21**, 2230 (1988).
- ³¹A. Baumgärtner, *Annu. Rev. Phys. Chem.* **35**, 419 (1984); in *Applications of the Monte Carlo Method in Statistical Physics*, edited by K. Binder (Springer-Verlag, Heidelberg, 1984), Chap. 5.
- ³²J. M. Deutsch, *Phys. Rev. Lett.* **49**, 926 (1982); **51**, 1924 (1983).
- ³³K. Kremer, *Phys. Rev. Lett.* **51**, 1923 (1983).
- ³⁴J. Skolnick and R. Yaris (private communication, 1988).
- ³⁵J. S. Higgins and J. E. Roots, *J. Chem. Soc. Faraday Trans 2* **81**, 757 (1985); J. S. Higgins, *Physica* **136B**, 201 (1986).
- ³⁶D. Richter, B. Ewen, B. Farago, and T. Wagner, *Phys. Rev. Lett.* **62**, 2140 (1989); D. Richter (private communication, 1989).
- ³⁷S. F. Edwards, *Proc. R. Soc. London, Ser. A* **385**, 267 (1982).
- ³⁸K. Iwata and S. F. Edwards, *J. Chem. Phys.* **90**, 4567 (1989).
- ³⁹W. W. Graessley and S. F. Edwards, *Polymer* **22**, 1329 (1981).
- ⁴⁰T. A. Kavassalis and J. Noolandi, *Phys. Rev. Lett.* **59**, 2674 (1987); *Macromolecules* **22**, 2720 (1989).
- ⁴¹D. E. Kranbuehl and P. H. Verdier, *Macromolecules* **17**, 749 (1984).
- ⁴²K. Kremer and K. Binder, *J. Chem. Phys.* **81**, 6381 (1984).
- ⁴³K. Kremer and K. Binder, *Comput. Phys. Rep.* **7**, 259 (1988).
- ⁴⁴K. Binder, in *Molecular Level Calculations of the Structure and Properties of Non-Crystalline Polymers*, edited by J. Bicerano (Dekker, New York, 1989).
- ⁴⁵M. Fixman, *J. Chem. Phys.* **69**, 1527 (1978); **69**, 1538 (1978); M. R. Pear and J. H. Weiner, *ibid.* **71**, 212 (1979); W. F. van Gunsteren, H. J. C. Berendsen, and J. A. C. Rullmann, *Mol. Phys.* **44**, 69 (1981); R. M. Levy, M. Karplus, and J. A. McCammon, *Chem. Phys. Lett.* **65**, 4 (1979); G. T. Evans and D. C. Knauss, *J. Chem. Phys.* **72**, 1504 (1980).
- ⁴⁶E. Helfand, *J. Chem. Phys.* **69**, 1016 (1978); E. Helfand, Z. R. Wasserman, and T. A. Weber, *ibid.* **70**, 2016 (1979).
- ⁴⁷R. W. Hockney and J. W. Eastwood, *Computer Simulations using Particles* (McGraw-Hill, New York, 1981).
- ⁴⁸*Molecular Dynamics Simulations of Statistical Mechanical Systems*, edited by G. Ciccotti and W. G. Hoover (North-Holland, Amsterdam, 1986).
- ⁴⁹M. P. Allen and D. J. Tildesley, *Computer Simulations of Liquids* (Clarendon, Oxford, 1987).
- ⁵⁰D. Fincham, *Mol. Simulation* **1**, 1 (1987).
- ⁵¹M. Bishop, M. H. Kalos, and H. L. Frisch, *J. Chem. Phys.* **70**, 1299 (1979); D. C. Rapaport, *ibid.* **71**, 3299 (1979); W. Bruns and R. Bansal, *ibid.* **74**, 2064 (1981); **75**, 5149 (1981); Yu. Ya. Gotlib, N. K. Balabaev, A. A. Darinskii, and I. M. Neelov, *Macromolecules* **13**, 602 (1980); P. G. Khalatur, Yu. G. Papulov, and A. S. Pavlov, *Mol. Phys.* **58**, 887 (1986).
- ⁵²G. S. Grest and K. Kremer, *Phys. Rev. A* **33**, 3628 (1986).
- ⁵³G. S. Grest, K. Kremer, and T. A. Witten, *Macromolecules* **20**, 1376 (1987); G. S. Grest, K. Kremer, S. T. Milner, and T. A. Witten, *ibid.* **22**, 1904 (1989).
- ⁵⁴M. Murat and G. S. Grest, *Macromolecules* **22**, 4054 (1989); *Phys. Rev. Lett.* **63**, 1074 (1989).
- ⁵⁵P. Flory, *Statistical Mechanics of Chain Molecules* (Interscience, New York, 1969).
- ⁵⁶J. Rudnick and G. Gaspari, *J. Phys. A* **19**, L191 (1986).
- ⁵⁷M. Bishop and J. M. J. Michele, *J. Chem. Phys.* **84**, 444 (1986).
- ⁵⁸J. Batoulis and K. Kremer, *Macromolecules* **22**, 4277 (1989).
- ⁵⁹M. Dial, K. S. Crabb, C. C. Crabb, and J. Kovac, *Macromolecules* **18**, 2215 (1985). Here the correction due to the chain end was not considered.
- ⁶⁰I. Carmesin and K. Kremer, *J. Phys. (Paris)* (in press).
- ⁶¹G. C. Berry and T. G. Fox, *Adv. Polym. Sci.* **5**, 261 (1968).
- ⁶²J. G. Curro, K. G. Schweizer, G. S. Grest, and K. Kremer, *J. Chem. Phys.* **91**, 1357 (1989).
- ⁶³S. Candau, J. Bastide, and M. Delsanti, *Adv. Polym. Sci.* **44**, 27 (1982).
- ⁶⁴T. A. Vilgis and S. F. Edwards, *Rep. Prog. Phys.* **51**, 243 (1989).
- ⁶⁵G. S. Grest and K. Kremer (unpublished).
- ⁶⁶R. Kimmich, G. Schnur, and M. Koerf, *Prog. NMR Spectrosc.* **20**, 385 (1988).
- ⁶⁷R. J. Needs, *Macromolecules* **17**, 437 (1984).
- ⁶⁸E. Douth, *Poly. Bull.* **7**, 417 (1982).
- ⁶⁹M. Doi, *J. Poly. Sci. Polym. Phys. Ed.* **21**, 667 (1983).
- ⁷⁰J. des Cloizeaux, *J. Phys. Lett.* **45**, L17 (1983).
- ⁷¹W. W. Graessley and M. Struglinski, *Macromolecules* **19**, 1754 (1986).
- ⁷²M. Antonietti, H. K. Foelsch, and H. Sillescu, *Makrom. Chem.* **188**, 2317 (1987); M. Antonietti, J. Contandin, and H. Sillescu, *Macromolecules* **19**, 793 (1986); H. Sillescu (private communication). For Fig. 22 and the mapping, we used only the data at the highest temperature, $T = 495$ K, since these data are far above the glass transition.
- ⁷³P. G. de Gennes, *Phys. (N. Y.)* **3**, 97 (1967).
- ⁷⁴B. Bernu, J. P. Hansen, Y. Hiwatari, and G. Pastore, *Phys. Rev. A* **3**, 4841 (1987).
- ⁷⁵D. S. Pearson, G. Verstrate, E. von Meerwall, and F. C. Schilling, *Macromolecules* **20**, 1133 (1987).
- ⁷⁶For PDMS, see Ferry (Ref. 3) for PTHF: D. S. Pearson (private communication); see also Ref. 35.
- ⁷⁷L. J. Fetters (private communication).
- ⁷⁸J. M. Deutsch and N. Goldenfeld, *Phys. Rev. Lett.* **48**, 1694 (1982).
- ⁷⁹Data of Ref. 36 compared to Ref. 76.
- ⁸⁰R. Needs, *Macromolecules* **17**, 437 (1984).
- ⁸¹C. W. Gear, *Numerical Initial Value Problems in Ordinary Differential Equations* (Prentice-Hall, New York, 1971).
- ⁸²M. O. Robbins, K. Kremer, and G. S. Grest, *J. Chem. Phys.* **88**, 3286 (1988).
- ⁸³L. Woodcock, *Chem. Phys. Lett.* **10**, 257 (1971); F. F. Abraham, S. W. Koch, and R. C. Desai, *Phys. Rev. Lett.* **49**, 923 (1982).
- ⁸⁴G. S. Grest, B. Dünweg, and K. Kremer, *Comput. Phys. Commun.* **55**, 269 (1989).
- ⁸⁵K. G. Schweizer, *J. Chem. Phys.* **91**, 5802 (1989); **91**, 5822 (1989).
- ⁸⁶D. Richter, B. Farago, C. Lartigue, L. J. Fetters, J. S. Huang, and B. Ewen, *Phys. Rev. Lett.* (in press).